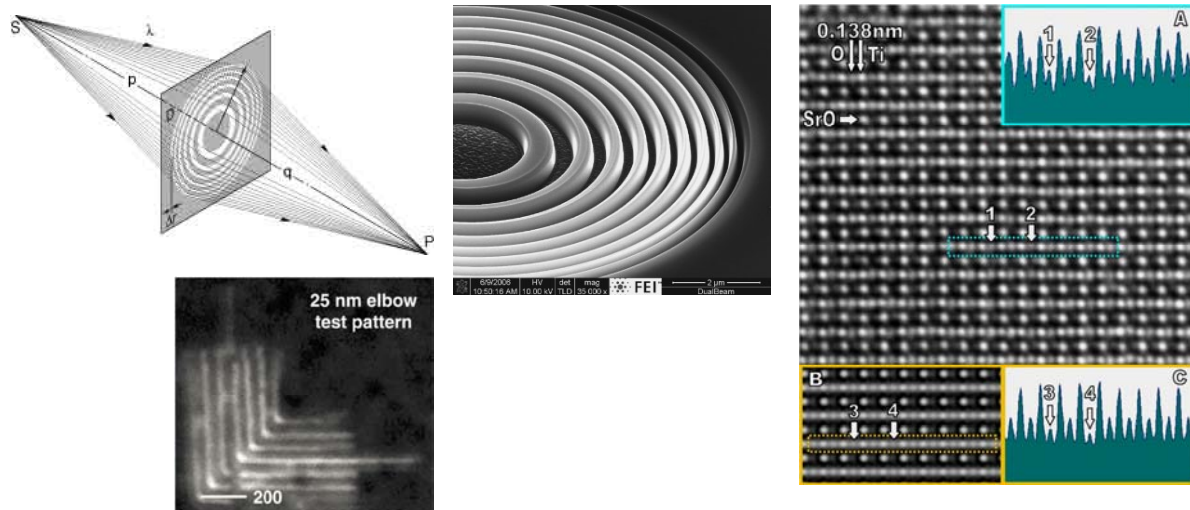# Chapter 7

X-Ray and Electron Microscopy

Optical Elements, Lens Aberrations and Resolution Limits

## Contents - Chapter 7

X-Ray and Electron Microscopy

7.1 Introduction

For *optical light microscopy* (see previous chapter) the best resolution is mainly given by the diffraction limit $r_{diff} = 0.61 \cdot \lambda / NA$ due to nearly perfect, high numerical aperture and aberration free optical systems.

» Thus, the best resolution of light microscopy is about half of the wavelength, i.e., $r_{best} \sim \lambda/2 \sim 200nm$

» *Shorter imaging wavelengths* are required to obtain higher spatial resolution: » *EUV, X-rays or electrons*.

X-rays: $\lambda \sim 1\ Å$; $r_{best} \sim 10 - 100\ nm$
(= **NA-limited** because α = small)

Electrons: $\lambda \sim 0.1 - 0.01\ Å$; $r_{best} \sim 1\ nm$
(= **aberration-limited** because of highly imperfect electron lenses)
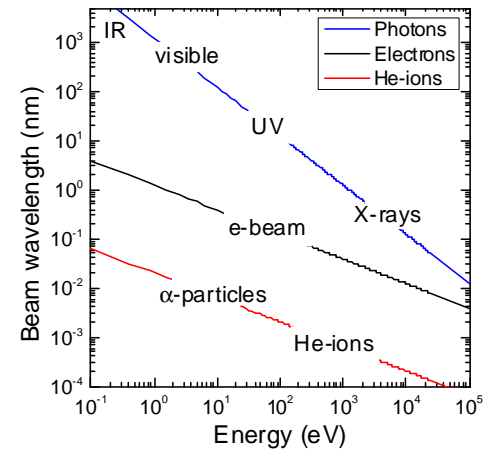
For these short wavelength probes, however, **no aberration free, high NA optical lenses exist**.

⇨ Thus, in this case the resolution is mainly *limited by the optics* and not so much by the wavelength, i.e., the best achievable resolution is $r \gg \lambda$.

Other complications:

● Normal refractive lenses do not work » alternative optical elements are required

● Small wavelengths mean high particle/photon energies (~keV). This means » different interaction and contrast mechanisms are present.

● The wavelength is comparable to interatomic distances » Diffraction at atomic lattices occur.

7.2 EUV & X-Ray Microscopy

To improve the resolution of optical microscopes, one could simply use EM radiation with shorter wavelength.
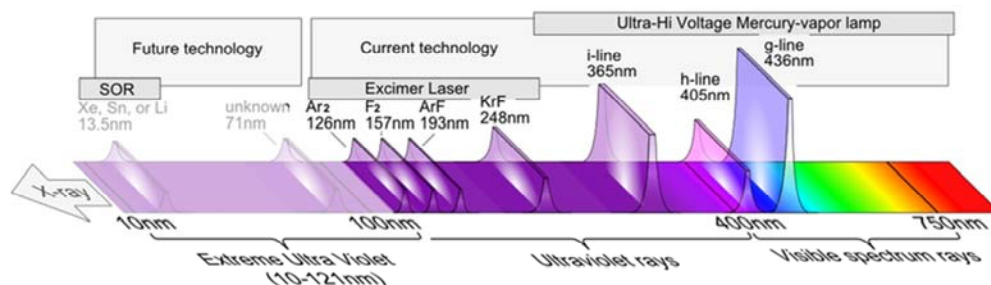
At short wavelengths, the *photon energy increases* beyond $E_{hv} > 10\ eV$ when $\lambda < 120\ nm$. As a result, the *light-matter interaction* of the photons drastically changes.

Resulting Problems:

1. Optical materials are *no longer transparent* because absorption always occurs (hv > W_A).

2. The refractive index of all materials approaches $n = 1$. Therefore, conventional *refractive* optics does not work in the UVU and XR regime, i.e. *different optics are needed* : Transition from refractive to *reflective* or *diffractive optics* !

3. Samples are no longer optically transparent. » EUV transmission microscopy possible only for very *thin specimen*. For reflection mode the reflectivity signal is small due to the small differences in the refractive indices of different materials ($n \sim 1$): $R_\perp = [(n-1)/(n+1)]^2$

4. **UV & VUV light is absorbed in air**: Vacuum required for VUV systems (but not for x-rays)

5. No readily available, cost effective light sources are available » plasma sources/synchrotrons

6. Damaging of optics and samples by irradiation can occur due to high photon energies.

7.2.1 Extreme UV Optical Systems

All solids, liquids, and gasses **absorb EUV photons**: Thus, EUV light is already completely absorbed in 100 nm of H_2O. As a result, *reflective* or *diffractive* **optical elements** are needed.

At short wavelengths, however, the **refractive index of all materials approaches $n \sim 1$**.
Thus, for all materials also the **reflectivity in the EUV is very small, i.e., R < 0.1 % !**

$$n(\omega) = 1 - \delta + i\beta \quad (3.12)$$

$$\delta = \frac{n_a r_e \lambda^2}{2\pi} f_1^0(\omega) \quad (3.13a)$$

$$\beta = \frac{n_a r_e \lambda^2}{2\pi} f_2^0(\omega) \quad (3.13b)$$

X-rays: $\delta \sim 10^{-4} - 10^{-6}$

$$R_\perp = [(n-1)/(n+1)]^2$$

- λ^2 behavior
- δ & β << 1
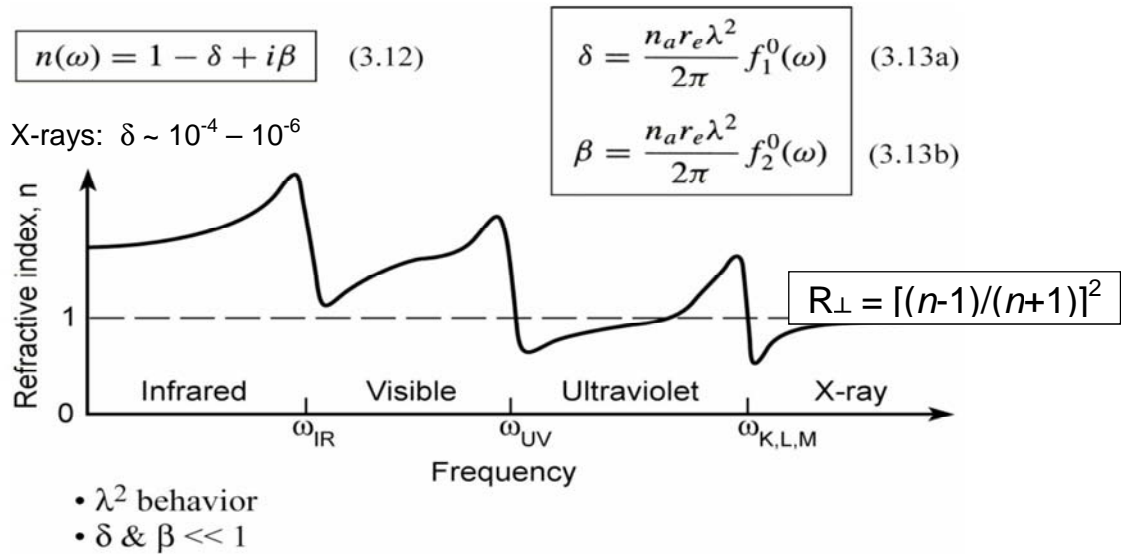
⇨ Therefore, a high reflectivity can be obtained only by the reflection at many interfaces using

multilayer *Bragg mirrors*. Such multilayers are designed such that the waves reflected at each interface interfere constructively with each other, such that the reflectivities of all interfaces add up.

Multilayer Bragg Mirrors

For EUV and soft X-ray optics, curved *reflective **Bragg mirrors*** consisting of many layers of e.g. molybdenum (high Z and high M_A) and silicon (low Z and low M_A) with maximum refractive index contrast are employed.

❖ ***Design*:** The individual layer thicknesses are designed such that the light reflected at each interface **interferes constructively** in backscattering geometry.

This means that the optical **thickness of each layer should be equal to λ/4** under normal incidence.

In the EUV where λ < 20nm this means that layer thicknesses well below 5 nm are needed.

Since for each single interface, the reflectivity is still very low $R < 1\%$, many periods are required to obtain a large total reflectivity.

In this way, EUV Bragg mirrors can reflect nearly 70 % of EUV light at 13.5 nm when the number of multilayer periods ($N > 50$) is large. Without coating, light would be almost totally absorbed.

❖ The **thicknesses** and compositions of all films must controlled to better than 1 nm.

N = 40
D = 6.7 nm λ = 13.4 nm

Ru   capping layer
Si
Mo
Si
Mo
Si
Mo

← B₄C

d

Substrate

Ru   (1.70 nm)
Si   (4.14 nm)
B₄C (0.25 nm)   d = 6.88 nm
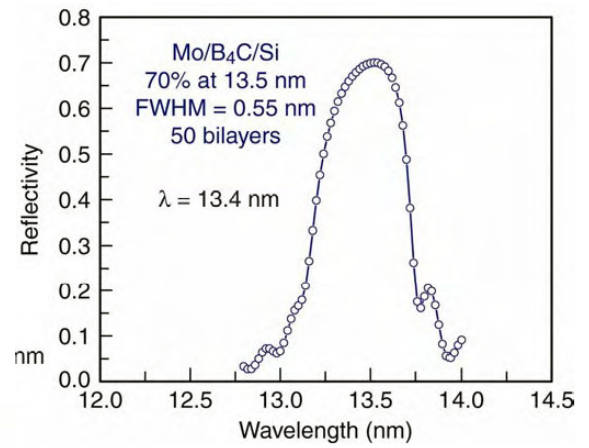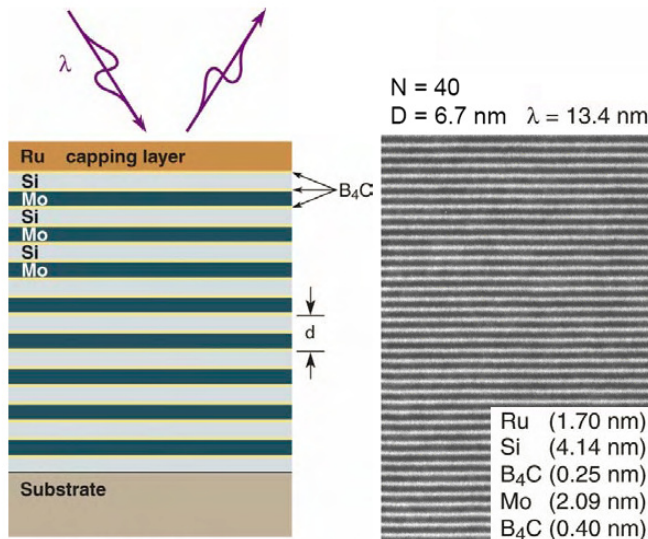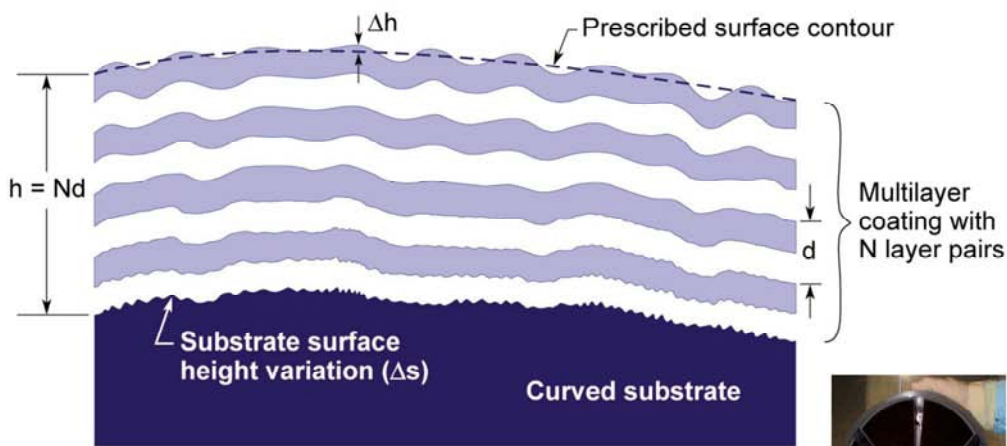Mo   (2.09 nm) Γ = 0.34
B₄C (0.40 nm)

Mo/B₄C/Si
70% at 13.5 nm
FWHM = 0.55 nm
50 bilayers

λ = 13.4 nm
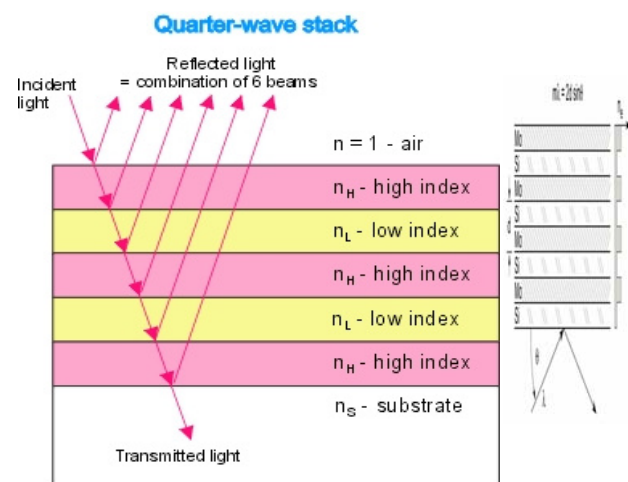
⇨ Mo/Si multilayer with N = 40 layer pairs:
  Yields ~70% reflectivity at 13.5nm where
  Mo and Si are most transparent.

⇨ For high reflection, the absorption should be
  low (i.e. attenuation length should be large).
  Mo, Si, Be are good candidates at λ~10-15nm.

In addition, the **mirror surfaces** have to be nearly perfectly flat with RMS roughness < 0.2 nm.
Even small defects in coatings can strongly degrade the quality of the mirrors.

Δh — Prescribed surface contour

h = Nd

Multilayer
coating with
N layer pairs

d

Substrate surface
height variation (Δs)

Curved substrate

$$\Delta h = \frac{1}{2\sqrt{5}\sqrt{N_S}}\frac{\lambda}{25}$$

$$\frac{\Delta d}{d} = \frac{1}{25\sqrt{5}\sqrt{N_S}\,N}$$

• $\frac{\lambda}{25}$ total rms wavefront error
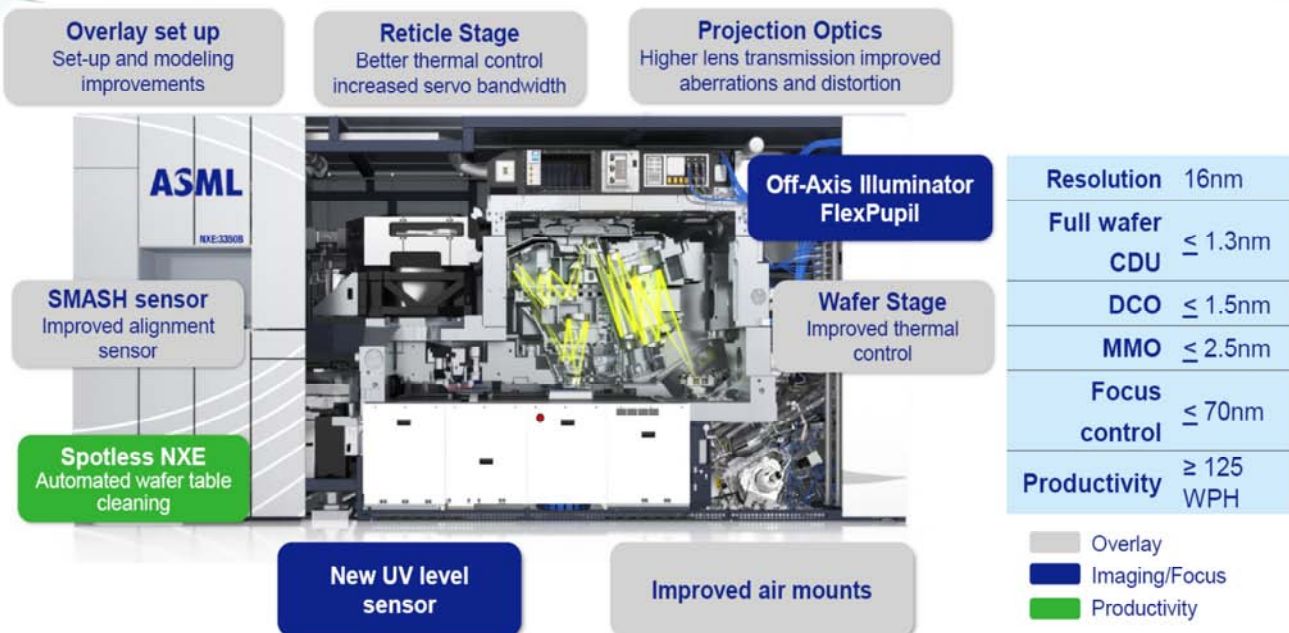• $\Delta h_{rms} = \Delta s_{rms}/2$
• double path in reflection

Condenser optic   Projection optic

⇨ EUV systems are very expensive and therefore the main current application is not for
  microscopy but actually EUV-lithography for fabrication of IC Si chips with <20nm feature size.

7.2.2 X-Ray Optics

(a) X-Ray Mirrors

⇨ Similar principle as for EUV **Bragg mirrors** can be also used for X-ray mirrors.

⇨ However, the **refractive index of x-rays is even closer to $n \sim 1$ for all materials.**
  » High reflectivity only for **grazing incidence angles** near the angle of total reflection ($\phi < 1°$)

⇨ Focusing action due to *curvature* of Bragg mirrors.

⇨

The Kirkpatrick-Baez mirror system

$\alpha < 1°$

» NA < 0.01

Resolution: $r_{diff} > 100 \, \lambda$
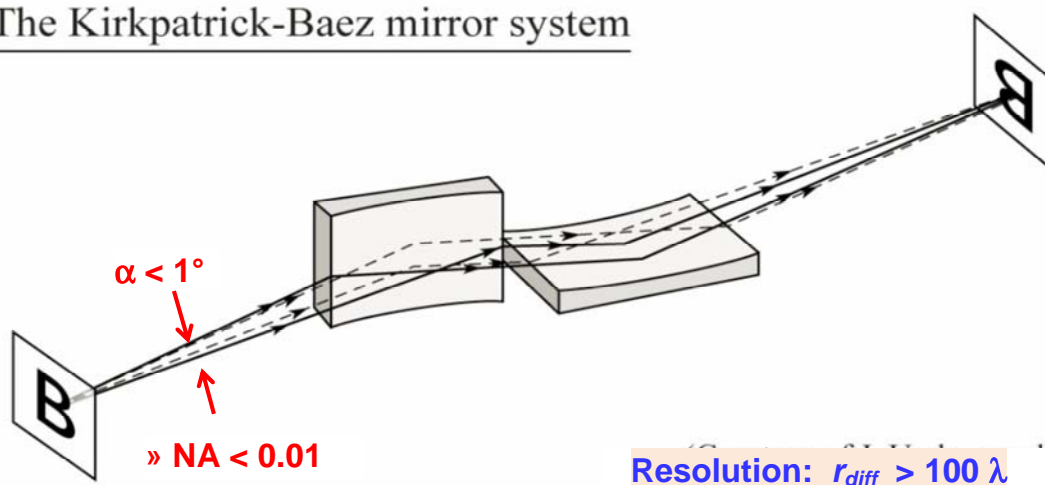
⇨ Very **demanding** and *expensive* due to very small layer thicknesses and surface roughness.

⇨ Small capture angles < 1° » *small numerical aperture NA* and thus, large diffraction broadening

(b) Diffractive Optics: Fresnel Zone Plates

Focusing optical elements can be also made based on *diffraction*.
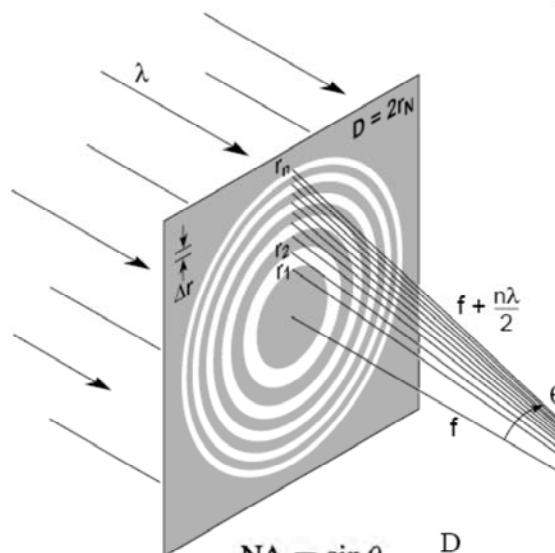
These elements are called **Fresnel zone plates** and consist of diffraction gratings with *graded* **line spacing** Δr that _decreases_ with increasing radius r from the optical axis.

$$f^2 + r_n^2 = \left(f + \frac{n\lambda}{2}\right)^2 \quad (9.8)$$

$$r_n = \sqrt{n\lambda f + \frac{n^2\lambda^2}{4}} \quad (9.9)$$

$$r_n \simeq \sqrt{nf\lambda} \quad (9.10)$$

$$f^2 + r_n^2 = \left[f + \frac{n\lambda}{2}\right]^2$$

$$r_n^2 = n\lambda f + \frac{n^2\lambda^2}{4}$$

Fresnel zone plate

2 μm
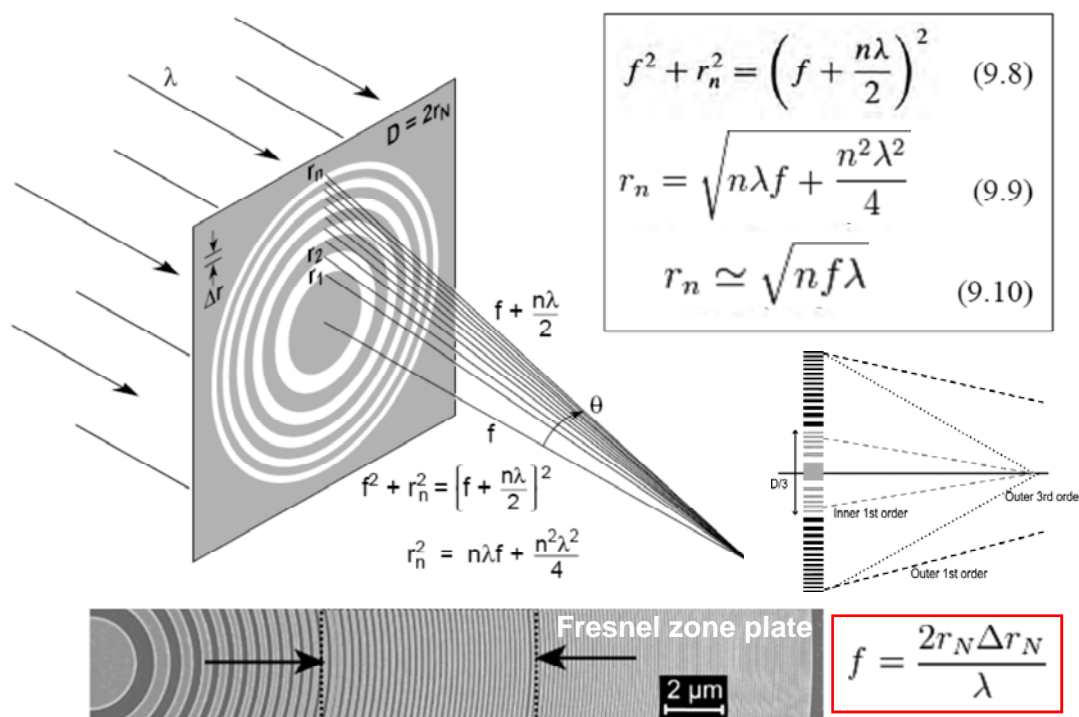
$$f = \frac{2r_N \Delta r_N}{\lambda}$$

SEM Images of X-Ray Fresnel Zone Plate

Define the outer zone width for n → N,

$$\Delta r \equiv r_N - r_{N-1} \qquad (9.11)$$

$$r_n^2 \simeq n\lambda f \quad \text{=last ring spacing}$$

$$r_N^2 - r_{N-1}^2 = N\lambda f - (N-1)\lambda f = \lambda f$$

$$r_N^2 - (r_N - \Delta r)^2 = 2r_N\,\Delta r - (\Delta r)^2 \simeq 2r_N\,\Delta r$$

$$2r_N\,\Delta r \simeq \lambda f$$

$$D\,\Delta r \simeq \lambda f \qquad (9.12)$$

but $\lambda f = \dfrac{r_N^2}{N} = \dfrac{D^2}{4N}$ (from 9.10)

$$\therefore \quad D\,\Delta r \simeq \frac{D^2}{4N}$$

$$\boxed{D \simeq 4N\,\Delta r} \qquad (9.13)$$

and from (9.12) above

$$\boxed{f \simeq \frac{4N(\Delta r)^2}{\lambda}} \qquad (9.14)$$

$$NA \equiv \sin\theta = \frac{D}{2f}$$

$$\boxed{NA \simeq \frac{\lambda}{2\,\Delta r}} \qquad (9.15)$$
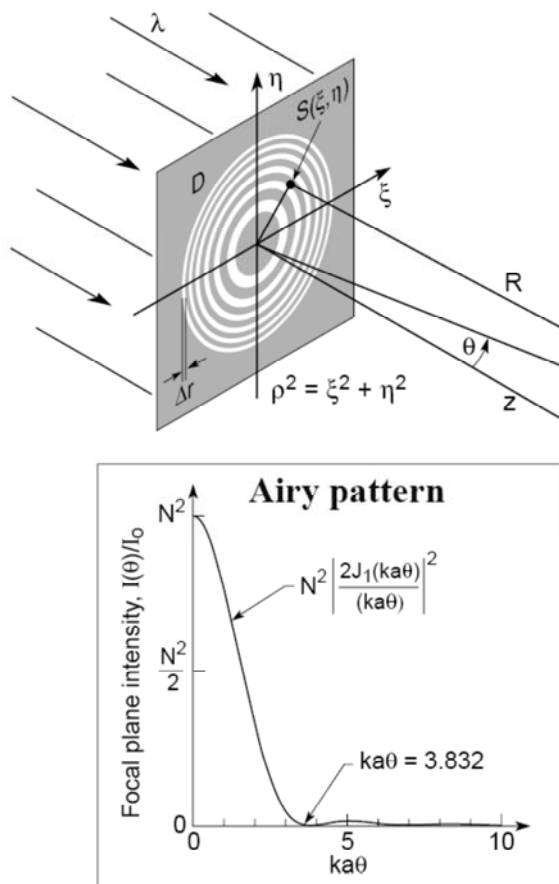
$$F^{\#} \equiv \frac{f}{D} \simeq \frac{\Delta r}{\lambda} \qquad (9.16)$$

Example: N = 100, λ = 1Å, Δr = 20nm » f = 1.64 mm

λ (~0.1 – 1 nm) << 2Δr (>20nm) » NA << 0.05 !!

⇨ **Diffraction limited resolution**: $r = 0.66\,\lambda\,/\,NA$ » **r ~ 50 nm**

$$\frac{I_1(\theta)}{I_0} = N^2 \left| \frac{2J_1(ka\theta)}{ka\theta} \right|^2 \qquad (9.45)$$

$$r_{\text{null}} = \frac{0.610\lambda}{NA} \qquad (9.46)$$

$$\boxed{NA \simeq \frac{\lambda}{2\,\Delta r}}$$

Airy pattern

$$\boxed{\text{Res}\big|_{\text{coh}} = \frac{0.61\,\lambda}{NA} = 1.22\,\Delta r}$$

⇨ Resolution determined by smallest outer ring spacing Δr of Fresnel lens (determined by fabrication process)

⇨ Actual resolution worse due to lens imperfections

7.2.3 X-Ray Microscopy Set-Ups

The most simplest and common approach is to use **scanning microscopy**, where a finely focused x-ray beam with a spot size of down to few 10 nm is scanned over a sample. Due to the small numerical aperture of x-ray focusing elements, the spot size and **resolution is > 100 λ**.

(a) Scanning transmission X-ray microscope (STXM)

(b) Full field transmission X-ray microscope (TXM)

Example: Scanning X-Ray Microscopy

Imaging of twin domains in Bi2Se3 and Bi2Te thin films using asymmetric Bragg diffraction.

Example: Coherent X-Ray Microscopy Imaging

Coherent x-ray imaging of domain boundaries within single GaN nanowires by coherent x-ray diffraction imaging and phase retrieval methods.

ACSNANO LABAT ET AL. VOL. 9 ▪ NO. 9 ▪ 9210–9216 ▪ 2015

Magnetic Recording Materials

100 nm lines & spaces →

Fe L_3 @ 707.5 eV

FeTbCo Multilayer
with Al Capping Layer
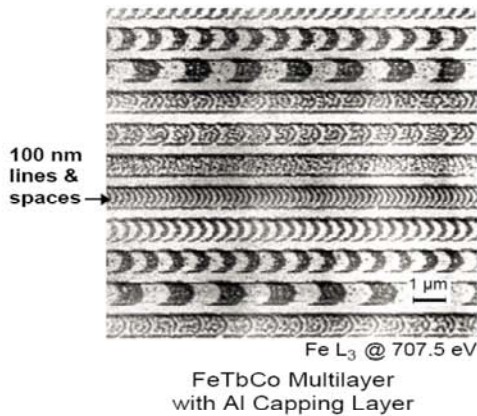
Courtesy of P. Fischer (Max Planck)
and G. Denbeaux (CXRO/LBNL)

Cryo Microscopy for the Life Sciences
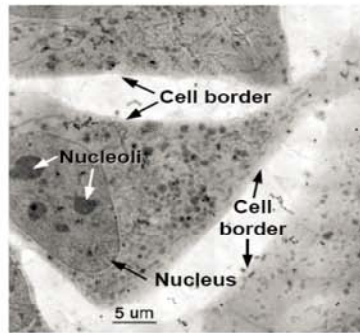
Cryo X-Ray Microscopy
of 3T3 Fibroblast Cells

Protein Labeled
Microtubule Network

Courtesy of C. Larabell (UCSF)
and W. Meyer-Ilse (CXRO/LBNL)

20 nm lines   14 nm lines   12 nm lines
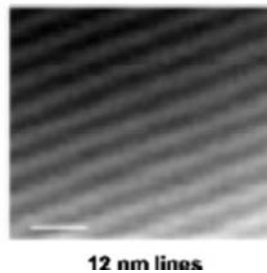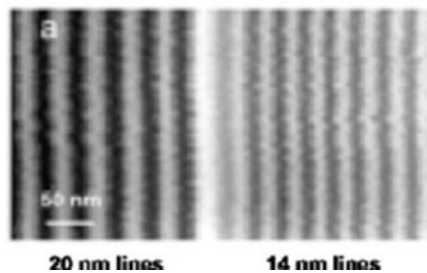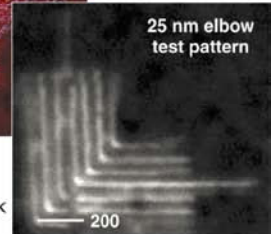
⇨ Resolution (= x-ray spot size) down to about 12 nm have been demonstrated !

7.3 Electron Microscopy

Electrons microscopes provide a very **high spatial resolution** down to ~ nm due to the orders of magnitude shorter wavelength of electron beams compared to visible light.

$$r_{diff} = 0.61 \cdot \lambda / n \sin \alpha$$

This drastically reduces the diffraction limit.

De Broglie wavelength of electrons: $\lambda_{electron} = \dfrac{h}{mv} = 1.225nm \big/ \sqrt{E(eV)}$ (E < 100keV)
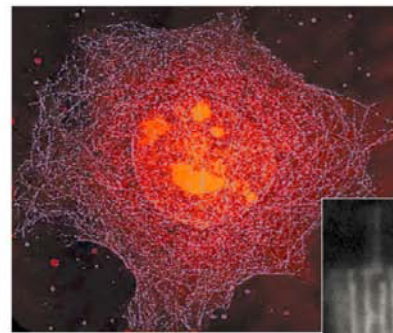
compare photon wavelength: $\lambda_{photon} = c / \upsilon = 1240 \; nm / E [eV]$ (E ~ 1-3eV)

Relativistic electrons: $\lambda_{rel} = h / [2 \, m_{0,e} \cdot E \, (1 + E/2 \, m_{0,e} \cdot c^2)]^{1/2}$ (E > 100kV).

⇨ For electron energies E > 150 eV the electron wavelength is λ <1 Å !

This also applies to protons or ion beams where λ << 1 Å already for E >1eV.

Comparison of Accelerating Voltage, Wavelength, and Resolving Power for a Transmission Electron Microscope		
As accelerating voltage increases, wavelength decreases and resolution decreases (improves).		
ACCELERATING VOLTAGE (V)	WAVELENGTH (nm)	RESOLUTION (nm)
20,000	0.0087	0.44
40,000	0.0061	0.31
60,000	0.0050	0.25
80,000	0.0043	0.21
100,000	0.0039	0.19
1,000,000	0.00087	0.10

Scanning electron microscope – SEM: E ~ 2 – 50 keV,
Transmission electron microscope – TEM: E ~ 50 – 300 keV

7.3.1 Representatives of Electron Microscopy

(1) Transmission Electron Microscopy (TEM) (~100 – 300 keV, typical)
Imaging using electron waves transmitted through thin sample slices using *magnification optics*.

= Analogon to optical imaging microscopy and thus, follows same principles and properties.

Features: Highest spatial resolution (~Å) and strong *diffraction contrast* because the electron wavelength is comparable or smaller compared to the interatomic lattice spacings. This results in very high sensitivity to structural properties, such as lattice defects, crystal structure and orientation, etc.

However: Electron transparent specimen required: Thickness less than about <100 nm.

(2) Scanning Electron Microscopy (SEM and STEM) (SEM: 2 - 50 keV. STEM: 10 – 200keV)
Imaging using a *focused electron beam* that is raster scanned across the sample.

SEM: Recording of the excited secondary and backscattered electrons. Imaging from above.

STEM: Recording of transmitted electrons or induced secondary electrons ejected during transmission of thin sample specimen (STEM = scanning transmission electron microscope).

Features: High sensitivity to surface morphology, large range of magnifications, large depth of focus.
Versatile and easy to use: No sample preparation needed (except for biological specimen).

(3) Low-Energy Electron Microscopy (LEEM) (~10 eV – 1000 eV)
Imaging using electron waves *reflected* from the samples.
Features: High surface sensitivity due to very low penetration depth of low energy electrons of <1nm. Many imaging and spectroscopy modes.

(4) Photo Electron Emission Microscopy (PEEM) (eV to 500 eV)
Imaging using photoelectrons emitted due to illumination with UV or X-ray light.
Features: High surface sensitivity due to small escape depth. Electronic structure.
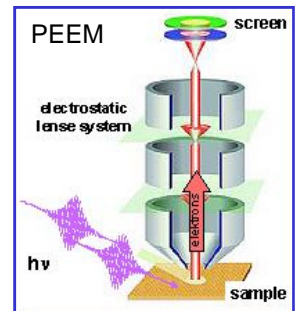
7.3.2 Basic Components

Electron microscopes consist of following components:

- **Electron source**: Electron gun and high voltage sources

- **Electro-optical column** with electron optics (magnetic or electrostatic lenses, beam deflection, apertures, ..)

- **Sample chamber** with movable and tiltable sample stage

- **Electron detectors** + optional x-ray detectors for chemical analysis

- **High vacuum system:** HV pumps, valves pressure gauges, …

- **Load lock chamber** for rapid sample exchange

- **Control electronics** & computer control system

- **Image analysis** and processing software

- **Sample preparation**: TEM: Thinning / cutting / polishing SEM: Conductive coating (Au, graphite , …)

SEM
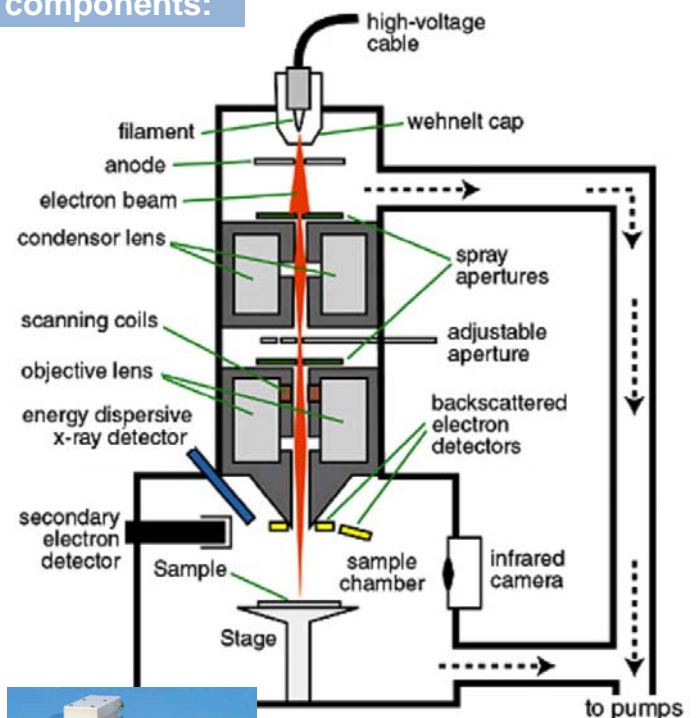
TEM
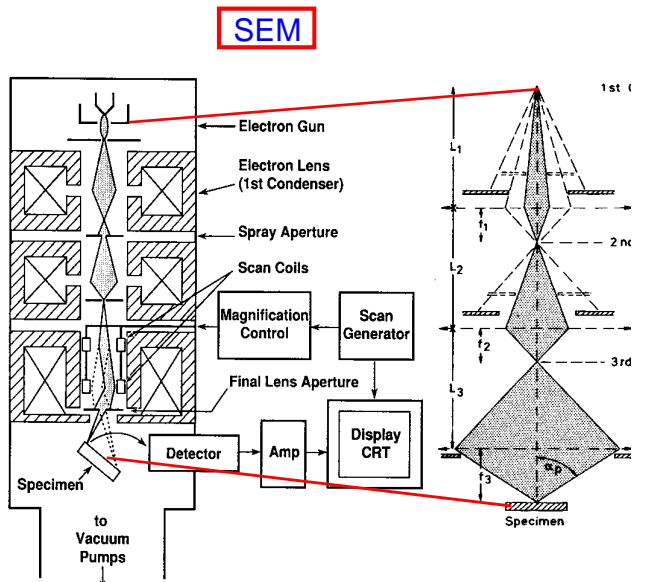
SEM set up and features:

- *Demagnifying* optics to produce small spot size.
- Detection of secondary / backscattered electrons.
- Sensitive to surface morphology and composition.
- Large sample sizes and thicknesses possible.
- Best resolution at intermediate/low e^- energy.
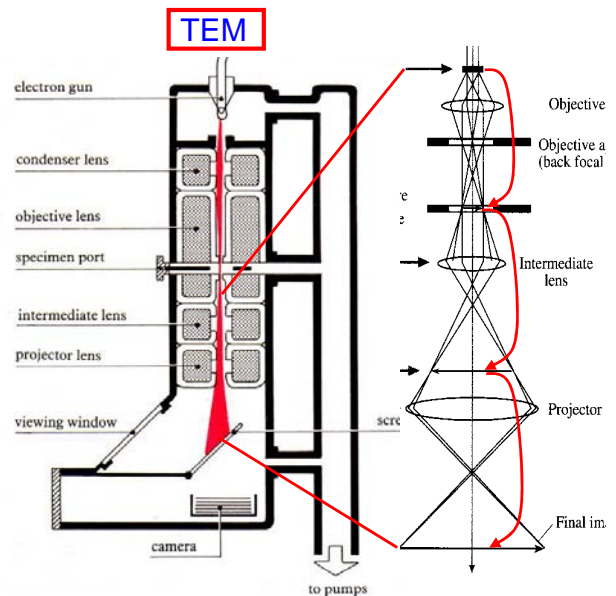
TEM set-up and features:

- *Magnifying* optics to produce enlarged image.
- Detection of transmitted electrons & waves.
- Strong diffraction effects, sensitive to structure.
- Electron-transparent thin sample slices required.
- Resolution increases with higher e^- energy.

Optical Diagram for TEM

TEM is the electron analog to an optical microscope, in which by magnification lenses a highly enlarged real image of the sample is produced on a viewing screen, in which the contrast reflects the probability that an electron impinging on a given spot on the sample reaches the detector.
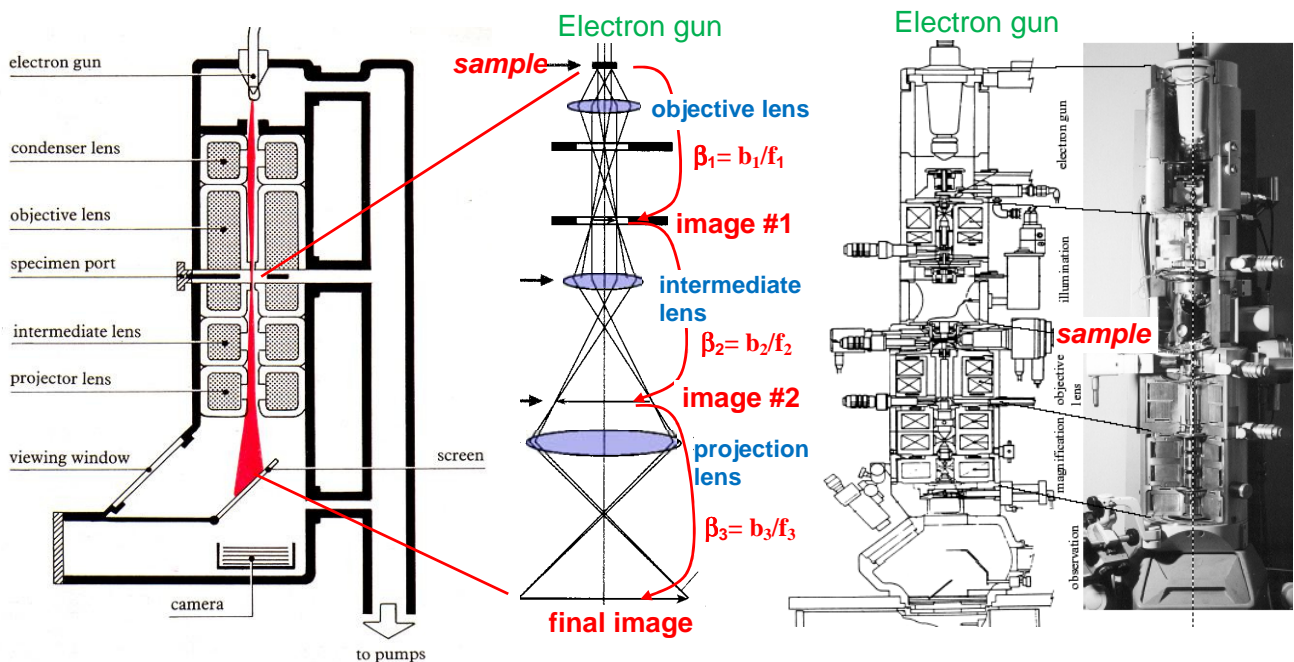
Magnification in each stage: $\beta_i \sim \beta_i / f_i$, from lens equation (see chapter 5)

Magnetic electron lenses: Focal length f_i can be varied continuously by changing the magnetic field strength.

Total magnification $\beta_{tot} = \beta_1 \times \beta_2 \times \beta_3$

Features of TEM

- TEMs are usually operated at high voltages ~ 50 -300keV to obtain the highest resolution and long transmission lengths. This requires considerably expensive high voltage components.

- The electo-optical column consist of a separate collimation and magnification lens systems.

- 2D detectors for image recording such a fluorescent screens or CCD cameras.

- Different imaging modes available that require additional apertures in the optical path.

- Transmission requires thin sample specimens: Difficult sample preparation.

Special features of TEM

1. The **image contrast** can be drastically changed using different apertures and imaging modes: Bright-field, dark-field, phase contrast, high-resolution mode, etc. ..

2. For TEM imaging, the **sample specimen** have to be thinned to few 100 nm or below to become electron transparent. Thinner samples yield higher spatial resolution. This requires special sample preparation techniques.

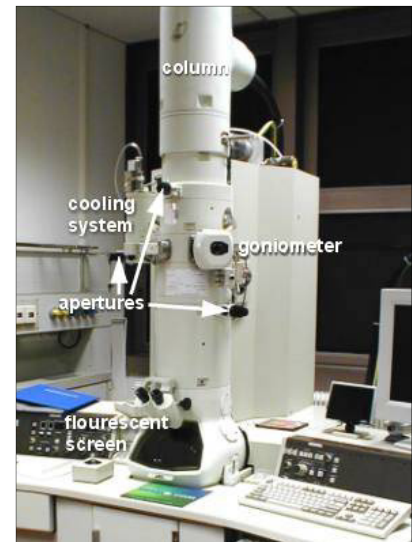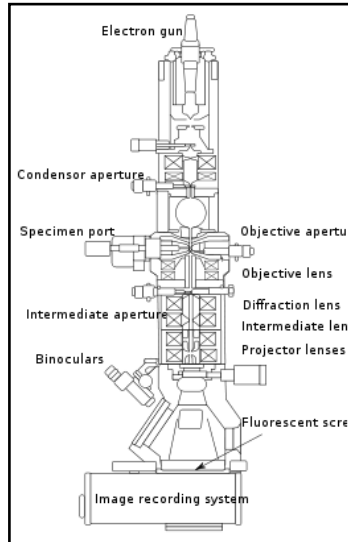3. **Higher resolution** is achieved down to 0.1 nm. This is mainly due to the higher electron energy as well as reduced electron sample scattering due to the thin sample thickness.

4. Apart from imaging, also local **electron microdiffraction** investigation can be performed for structure analysis.

5. **Energy filtering** as well as electron energy loss spectroscopy (EELS) can be applied to obtain chemical contrast images.

6. Apart from parallel imaging, TEM can be also operated in a **scanning transmission electron microscopy mode** (STEM), where the electron beam is tightly focused and scanned across the sample like in a SEM. The transmitted, scattered or induced secondary electrons can be detected by additional detectors positioned close to the sample.

High resolution TEM

Cu grains   diffraction

EELS imaging of MOS transitor

Red=O. Green=N. Blue=Si
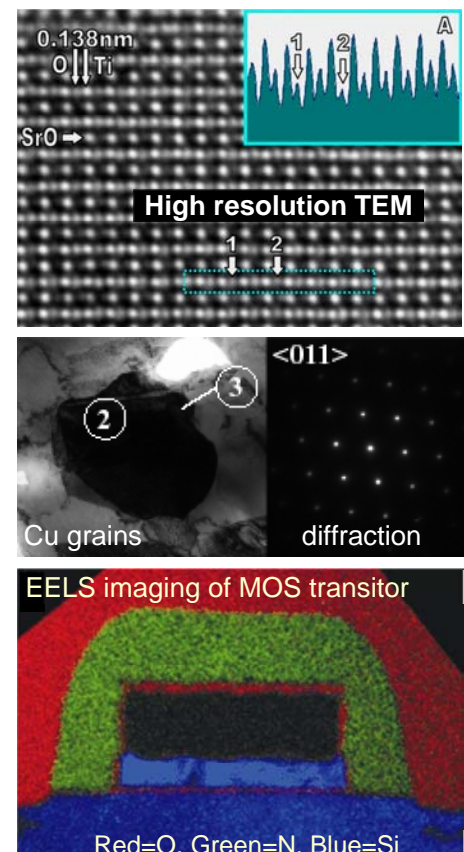
7.4.1 TEM Modes: Diffraction

The TEM image is typically formed by a three magnification lenses between the object and screen. Depending on the settings of the intermediate lens, two types of imaging modes can be obtained.

A. Diffraction mode

At the back focal plane of the objective lens diffracted *parallel beams* from the sample are focused on the same point and thus, diffraction pattern of the electrons is formed.

If the focal length of the inter-mediate lens is set such that this diffraction pattern is projected on the second intermediate image, the dif-fraction pattern is magnified onto the viewing screen.
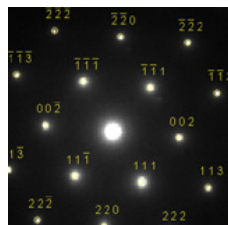
Electron diffraction pattern

B. Imaging mode

To produce a *real image* of the sample, the intermediate lens is set such that the real intermediate image 1 that is formed at the image plane of the objective lens is projected onto the object plane of the final projector lens, which is then magnified onto the final viewing screen.

A

Diffraction mode   **Imaging mode**

B

Specimen

Objective lens

Diffraction pattern

Objective aperture (back focal plane)

Fixed

SAD aperture

Intermediate image 1

Change strength

Intermediate lens

Second intermediate 'image'

Fixed strength

Projector lens

Diffraction pattern

Final image

Screen
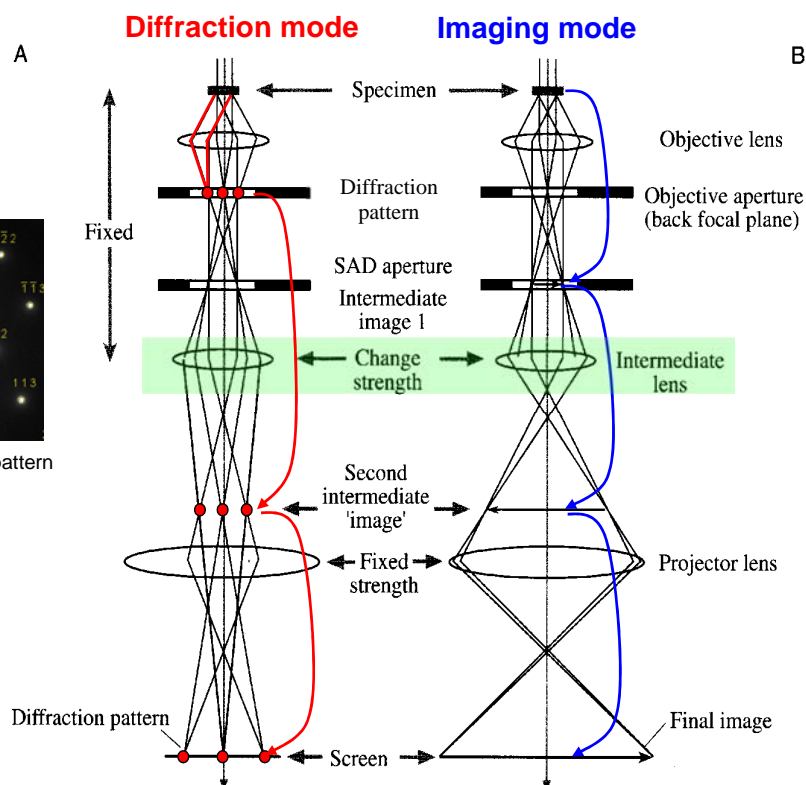
⇨ In TEM, by changing the focal length of the intermediate lens, one can choose between the diffraction pattern (back focal plane) or the image (in the image plane).
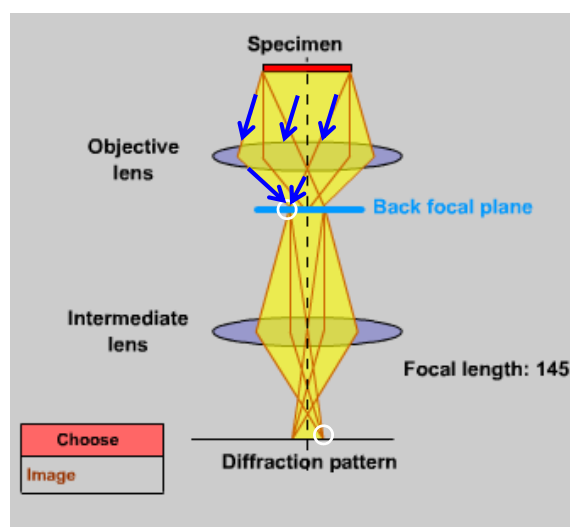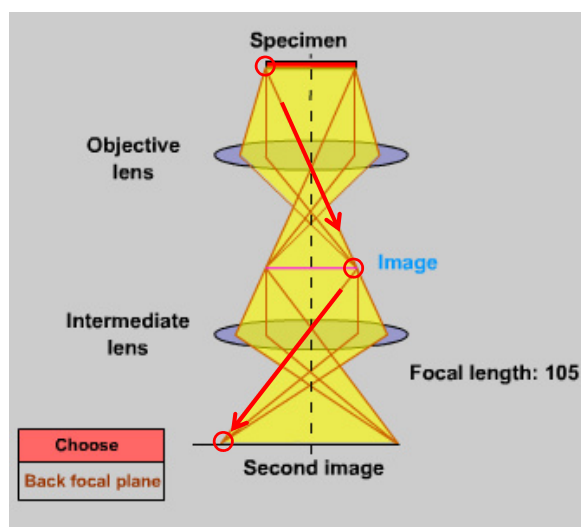
The diffraction pattern is highly useful for obtaining local structural information as well as for orienting the sample, as well as to obtain diffraction contrast images in the so-called dark-field or bright field imaging modes using small apertures inserted in the back focal plane.

Example:

Diffraction contrast in the bright field mode for a thin Ti- foil:

Make dislocations and crystal defects visible in the selected sample area.

Fig. 4.10. a) experimental illustration of in-focus and out-of-focus images of a Ti foil, recorded with no apertures inserted in the column; b) the selected area aperture is placed at the dashed circle in the center image of a), and the image inside the aperture is focused; c) switching to diffraction mode, a diffraction pattern is obtained (in this case near [01.0] zone axis orientation); d) the diffraction aperture is inserted around the central beam, and e) in image mode a high
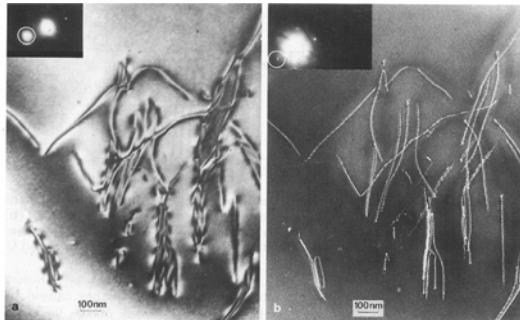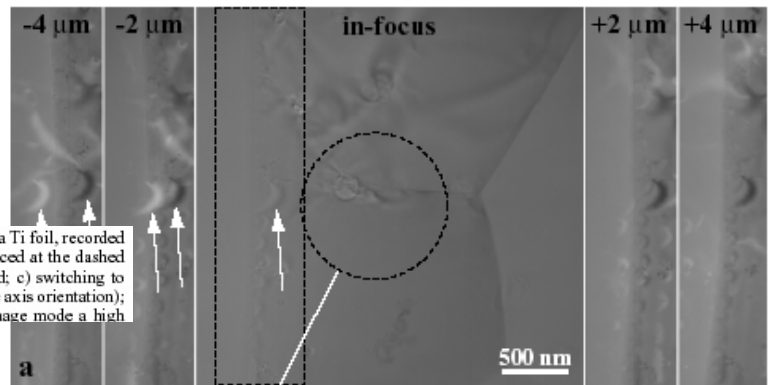
Fig. 9.24. (a) Dislocations in heavily deformed silicon imaged with a strong $2\bar{2}0$ diffracted beam. (b) Weak-beam $2\bar{2}0$ dark-field image of the same area showing the increase of the resolution of dislocation detail. The insets show the diffraction conditions used to form the images [9.91]

7.4.3 TEM Resolution

Because the aberrations of electron lenses are very larger, i.e., $r_{aber} > r_{diff}$ the *practical resolution* of is mostly limited by lens aberrations.

$$r_{eff} = (r^2_{dif} + r^2_{aber})^{1/2}$$

Electron Lenses

Electrons can be deflected by electric *or* magnetic fields, but **magnetic fields** are generally more effective at high electron energies because the Lorentz force increases with electron velocity.

For a focusing action, a **nonuniform radially varying B-field distribution** is required such that outer electrons are bend more strongly towards the optical axis than near-axis electrons.

Such a nonuniform magnetic field is produced by the stray field of a coil surrounded by a iron pole piece that is interrupted by a gap in the central bore.

Since the field strength can be changed through the applied voltage or current, the focal length of electron lenses can be continuously adjusted.

$$\vec{F}_L = e \cdot \vec{v} \times \vec{B}$$
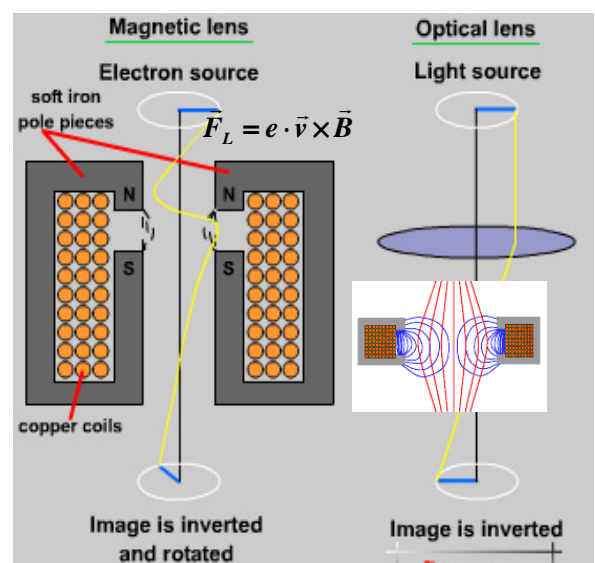
Aberrations: Due to the non-ideal magnetic
field distribution, electron lenses exhibit very large intrinsic lens aberrations.

Due to these aberrations, the aperture angles of electron lenses must be kept very small, in order to limit the effect of lens errors, which rapidly increases with α^n. Typically $\alpha \leq 0.3°$!

$\Rightarrow$ Achievable NA is much smaller than for optical lenses:

$$NA_{TEM} \sim 0.005 \quad \Rightarrow \quad r_{eff} \sim 100 \lambda$$

7.4.4 Principle of Magnetic Electron Lenses

Magnetic lenses consist of a *coil* with a central bore, surrounded by a soft iron *pole piece* that is interrupted by a *gap* within the bore. This creates a *nonuniform magnetic field distribution*.

The magnetic field strength and thus, the focal length of the lens can be adjusted by the *coil current*.

The focusing action is based on the inhomogeneous magnetic field distribution: Along the optical axis, the B-field is parallel to the z-axis and **Bell-shaped**:

$$B_z(z) = \frac{B_0}{1+(z/a)^2}$$

B_0 is the maximal center field and $2a$ the FWHM.

For on-axis electrons, the velocity is parallel to z and therefore, the Lorentz force and deflection is zero.

Away from the optical axis, the radial magnetic field B_r can be deduced from the Gauss law (div B = 0):

$$\pi r^2 B_z(z) - \pi r^2 B_z(z+dz) - 2\pi r\, B_r\, dz = 0$$

and $B_z(z+dz) = B_z(z) + (\partial B_z / \partial z)\, dz + \dots$

$$\Rightarrow \quad B_r \approx \frac{-r}{2}\frac{\partial B_z}{\partial z} = \frac{r \cdot z \cdot B_0}{\left[1+(z/a)^2\right]^2}$$

because *B* is radially symmetric and $B_\varphi = 0$.
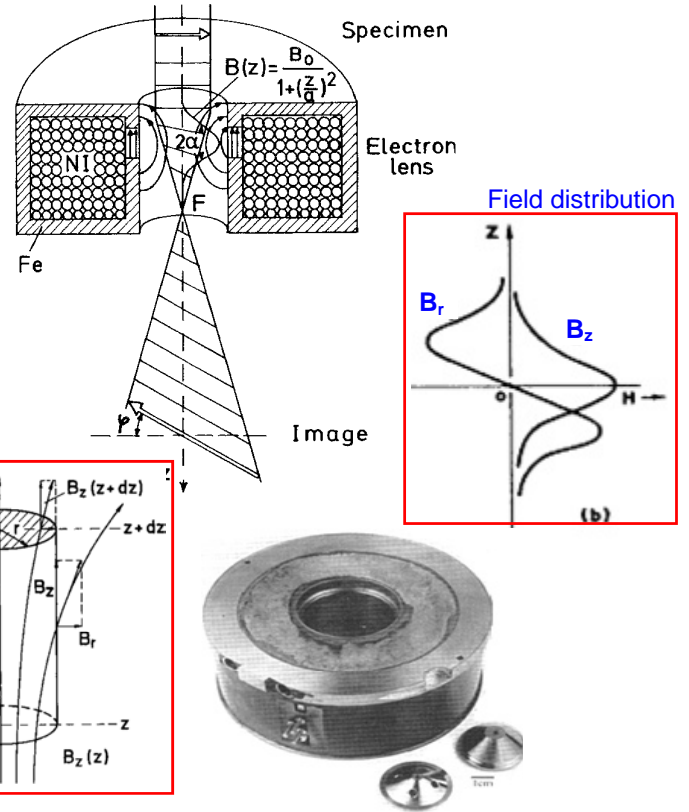
As a result of the nonuniform field distribution, the off-axis electrons experience a deflection force directed towards the central axis: It is given by the **Lorentz force**: $F_L - ev \times B$.

Focusing force and motion of the electrons: Using cylindrical coordinates (r,φ,z):

Radial component: $m\ddot{r} = F_r + mr\dot{\varphi}^2$ (1)   with the Lorentz force: $F_r = -e \cdot B_z \cdot v_\varphi = -e \cdot B_z \cdot r \cdot \dot{\varphi}$ (2)

Angular component: $d(mr^2\dot{\varphi})/dt = d(e \cdot r^2 B_z / 2)/dt$ (3)

$$\Rightarrow \quad \dot{\varphi} = \omega_L = e \cdot B_z / 2m \quad (4) \text{ where } \omega_L \text{ is the Larmor frequency.}$$

z - component: $m \cdot \ddot{z} = F_z \approx 0$ (5)   i.e., v_z ~ constant.

Inserting (4) and (2) in (1) yields the *focusing force* of

$$F_r = m\ddot{r} = -\frac{e^2}{2m} \cdot r \cdot B_z^2$$

towards the optical axis: ***F_r ~ r*** !!

Because this force increases with increasing *r*, the outer electrons are deflected stronger than the inner electrons. This yields a *focusing action* similar as for a optical lenses.

The resulting electron trajectories within a magnetic lens are shown in the graph on the right hand side as a function of the *lens strength ω*:

$$\omega = \sqrt{1+k^2} \quad \text{where} \quad k^2 = B_0^2 a^2 / 8 m_0 E_{el}$$

Fig. 2.7. Electron trajectories incident parallel to the axis for increasing values of lens strength $\omega = \sqrt{1+k^2}$ [2.2]

7.4.5 Aberrations of Electron Lenses

The focal points of electrons incident at different distance from the optical axis *r* are not on the same point. <u>Magnetic lenses</u> therefore exhibit rather <u>large lens aberrations</u>:
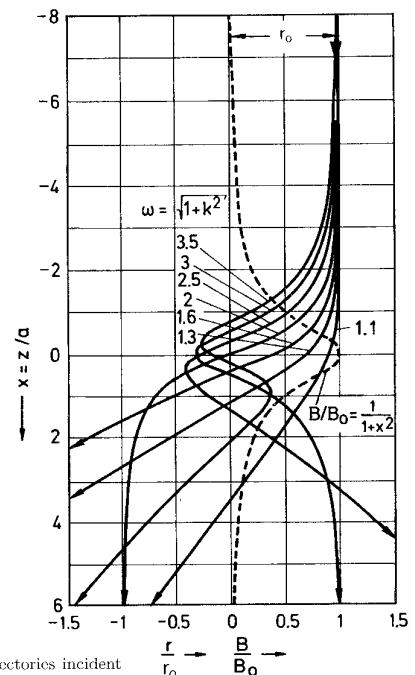
(i) Spherical Aberration: (Parallel beams are not focused exactly on the same focal point).

» **Broadening of the spot size** r_{sph} in the focal plane. Increases with α:

$$r_{sph} = C_s \alpha^3$$

» **Spherical aberration constant** are typically $C_s \sim$ **mm** for TEM lenses, increases with increasing lens strength proportional to the focal length.

Example: For C_s = 3mm => (i) α = 1° (12 mrad) $\rightarrow$ r_{sph} = 5 nm ;   (ii) α = 5° (87 mrad) $\rightarrow$ r_{sph} = 2 µm

(ii) Chromatic Aberration:

(Slower electrons are bend more strongly than faster electrons)

» Resulting broadening of the spot size (spot radius r_{chr}) is given by:

$$r_{chr} = C_c \frac{\Delta E}{E_0} \alpha$$

» **Chromatic aberration constant** $C_c \sim$ **mm**, increases with decreasing lens strength.

Although the energy spread of the primary electrons is typically smaller than 2 eV, the energy spread ΔE of the electrons transmitted through the sample is much larger (15 – 25 eV) due to inelastic scattering. ΔE increases with increasing sample thickness, i.e., chromatic errors increase.

(ii) Astigmatism: When the pole pieces are not perfectly symmetric and the optical axis not perfectly aligned, the electrons experience a non-uniform not radially symmetric magnetic field:

$$r_{ast} = \alpha \Delta f$$

Scherzer Theorem: Aberrations are **intrinsic** for rotational symmetric magnetic lenses and can in principle only be corrected by use of complicated **multipole lenses**.

7.4.6 Resolution due to Lens Aberrations and Diffraction

For any nonperfect lens system, the <u>resolution is limited</u> by
(i) <u>diffraction</u> where $r_{diff} \sim 1/\sin\alpha$,   as well as by (ii) <u>lens aberrations</u> where $r_{aber} \sim \alpha^n$,

Total effective resolution is given by:

$$r_{tot} = (r_{diff}^2 + r_{shp}^2 + r_{chr}^2 + r_{ast}^2)^{1/2}$$

$$r_{diff} = 0.61 \cdot \lambda / n \sin \alpha$$

Using $\sin\alpha \approx \alpha$, this yields:

$$r_{tot} = [(0.61 \cdot \lambda / \alpha)^2 + (C_{sph} \cdot \alpha^3)^2 + (C_{chr} \cdot \Delta E/E \cdot \alpha)^2]^{1/2}$$

α = aperture angle. C_{sph} and C_{chr} = spherical and chromatic lens aberration constants.

⇨ **With increasing aperture** α the diffraction broadening decreases but the broadening due to the lens aberration increases.

⇨ When the lens aberrations cannot be neglected, there exists a certain **optimum aperture angle** α_{opt} where the **highest resolution** is achieved !

⇨ This **applies to all microscopy methods**.

Figure: Resolution of an electron microscope as a function of aperture angle due to (i) diffraction, (ii) spherical aberration, and (iii) chromatic aberration. Calculated for *E* =300 keV, $\Delta E_{unfiltered}$= 250 eV, $\Delta E_{filtered}$= 30eV, C_s = 3.2 mm, C_c = 3.0 mm, and f_{obj} = 3.9 mm.

Resolution factors versus aperture angle

$r_{chr} \sim \alpha^1$

$r_{diff} \sim \alpha^{-1}$

$r_{sph} \sim \alpha^3$
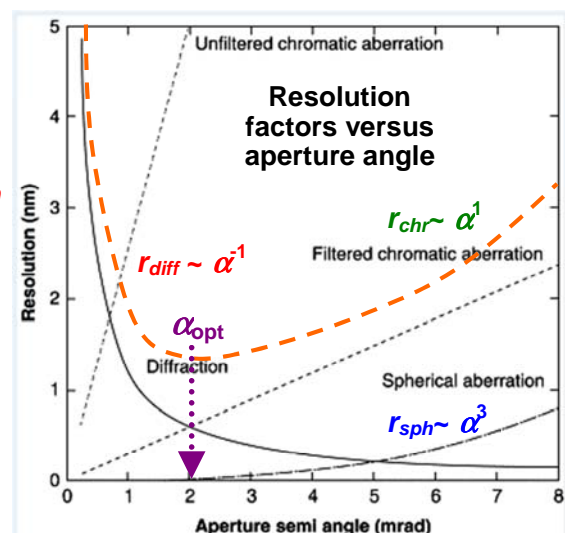
TEM Resolution

plotted as a function of:

- aperture angle α,
- spherical aberration C
- electron energy E

$$r_{tot} = \sqrt{r_{diff}^2 + r_{sphr}^2 + r_{chr}^2}$$

⇨ **Maximum (best) resolution (w/no C_{chr})**

= Minimum of r_{tot} neglecting chromatic & astigmatic aberrations

$$\mathbf{d}r_{tot}/\mathbf{d}\alpha = 0 \rightarrow \alpha_{opt} = 0.77 \text{ mrad} \cdot (\lambda / C_{sph})^{1/4} \quad \text{and} \quad \boxed{r_{best} = 0.91 \cdot (C_{sph} \cdot \lambda^3)^{1/4}} \text{ at } \alpha = \alpha_{opt}$$

Example: 200 keV, $\lambda = 0.0274$ Å, $C_{sph} = 0.5$ mm: » $\alpha_{opt} = 6.6$ mrad $= 0.38°$ » $\underline{r_{best}} = 2.9$ Å

With chromatic aberration: $C_{chr} = 2$ mm & $\Delta E = 20$ eV @ 200 keV: At $\alpha_{opt} = 6.6$ mrad » $\underline{r_{eff}} = 13.5$ Å

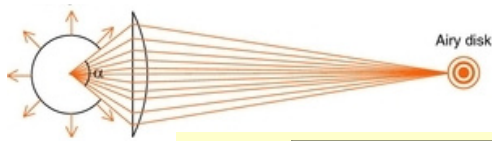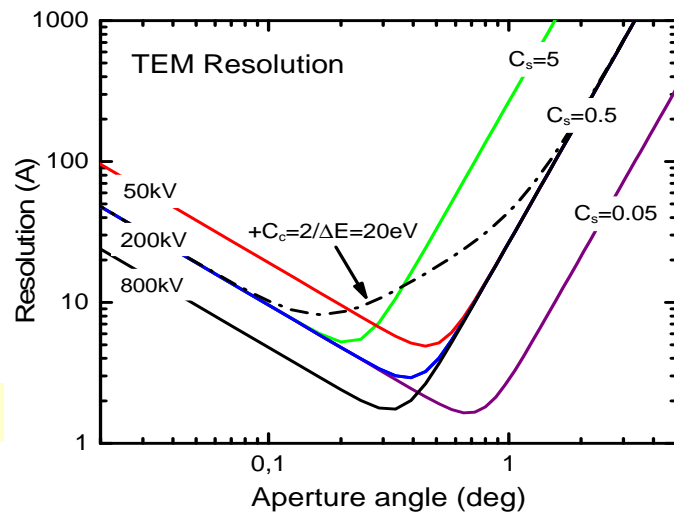- Chromatic aberration broadening is minimized when (i) using higher electron energies (smaller $\Delta E/E$) and (ii) for thin as possible specimens. This is essential for high resolution !
- From Bethe equation: dE/dx = 1… 3 eV per nm for 100 keV electrons (depending on material) !

7.4.7 Ultra-High Resolution TEM with Sub-Ångström Resolution

TEM Resolution is mainly limited spherical aberration: $r_{min} = 0.91 \cdot (C_{sph} \cdot \lambda^3)^{1/4}$

» Resolution can be improved only by   (a) decreasing the wavelength (=MeV TEMs) and/or

(b) and/or improveming the lens optics (aberration corrections).

Aberration corrections:

Scherzer (1936): Spherical aberrations cannot be avoided using rotationally symmetric fields !

Rose (1990ies): Spherical aberration corrections possible by using multipole fields that produce *negative* third order spherical aberrations for compensation.

» Development of hexapole and octopole correction lenses that can reduce C_{sph} to almost zero.

Additional measures for HR-TEM:

- Introduction of energy filters in the condenser system to improve the monochromaticity of the electron beam and thus reduce chromatic aberrations.
- Post sample energy filter (Omega filter
- Improved mechanical construction to reduce vibrations and thermal drifts of the TEM column.
- Improved stability and reduction of noise level of lens and gun currents.
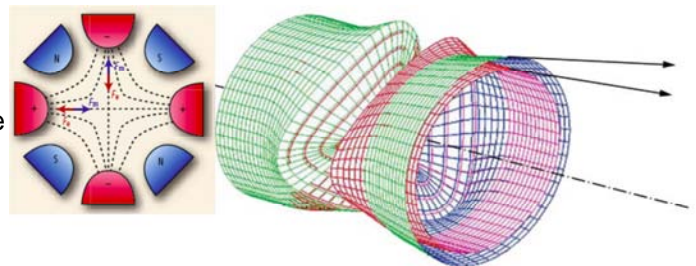
Figure 2 : Ray path through the hexapole Cs-corrector consisting of two hexapoles (rectangular boxes), which are separated by a telecentric round lens couple. It can be seen that the outer ray-path (green) is tilted away from the optical axis in order to compensate for the spherical aberration of the objective lens. Figure courtesy of Dr. S. Uhlemann, CEOS GmbH.

Resolution of Aberration Corrected TEM with Multipole Correction Lenses

C.L. Jia, M. Lentzen and K. Urban, Science 299, 870 (2003).

Multipole Correction Lenses yields C_s values as low as μm

Sub-Ångstrom resolution can be achieved by modern aberration corrected ultra-high resolution TEMs !
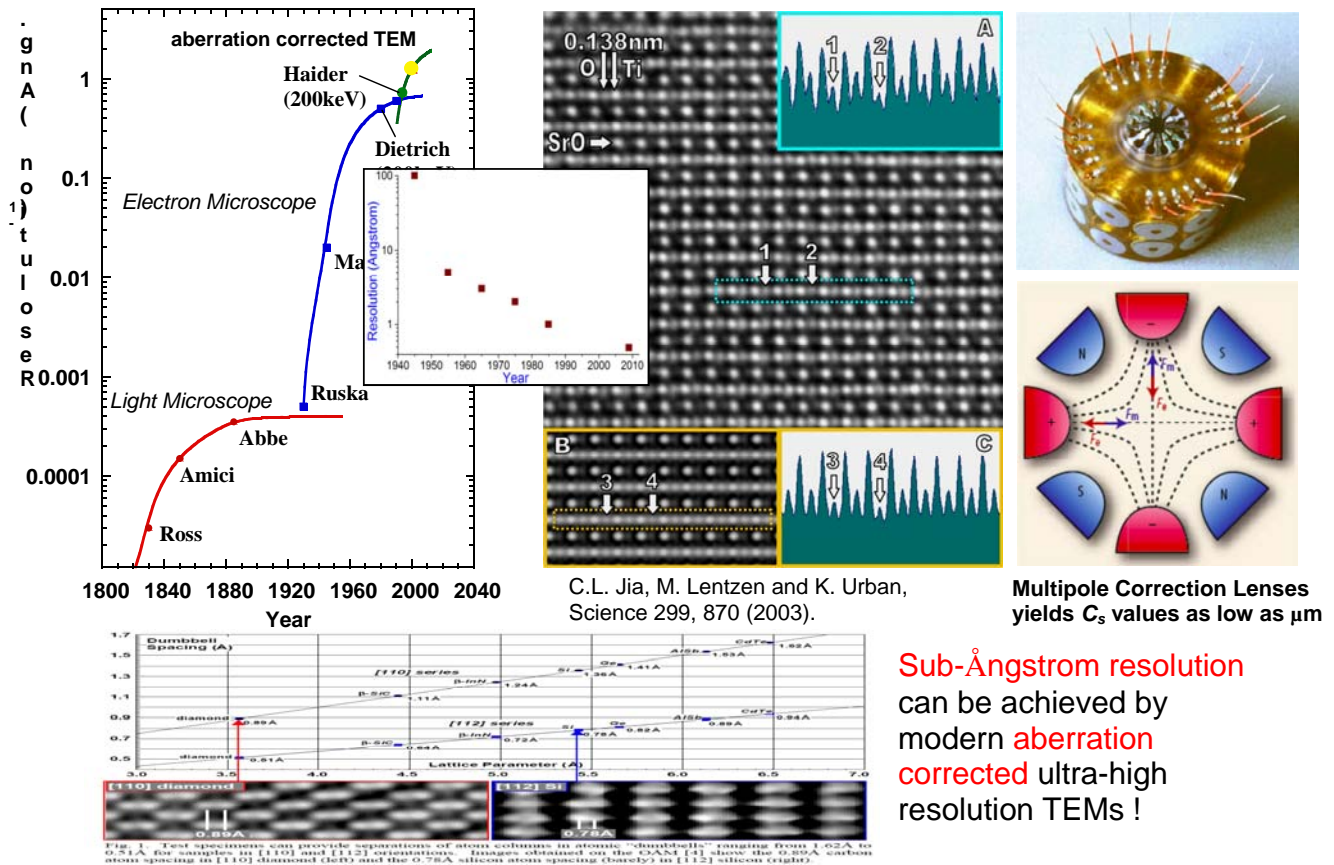
7.5 Scanning Electron Microscopy - SEM

- In SEM, the sample is raster *scanned* with a sharply *focused electron beam* of a few nm diameter and energy of 5 - 50 keV. The *magnification M* is the ratio between **scan size /display size**.

- **SEM images** = Lateral intensity distribution of **backward *emitted secondary electrons*** or of the ***backscattered electrons*** recorded as a function of the beam position on the sample. Alternatively, the excited x-ray photons, luminescence or sample current images can be recorded.
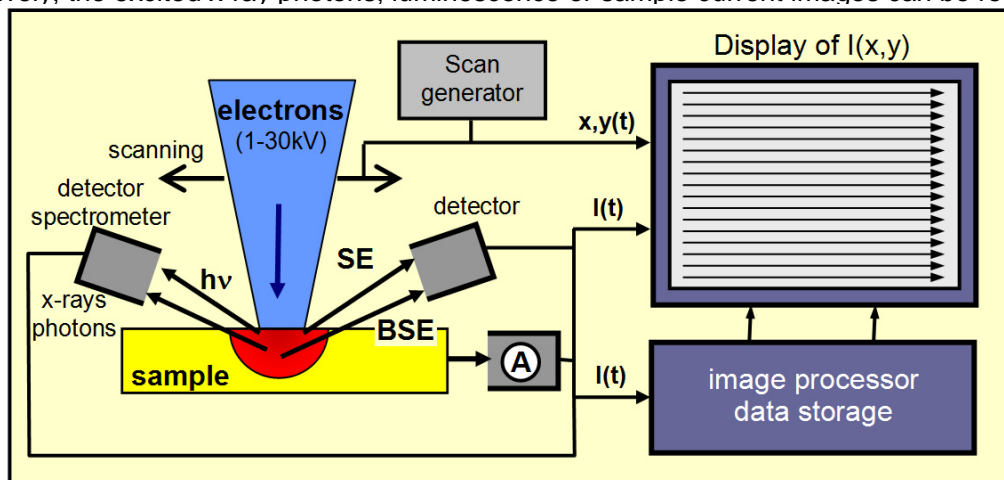
Features: High resolution (~few nm), no sample preparation needed, chemical analysis & spectroscopy

⇨ **Resolution** depends on probe size and interaction volume. Trend towards lower electron energies.

⇨ **Contrast** depends on the interaction mechanisms, beam parameters and detection schemes.

7.5.1 Instrumentation
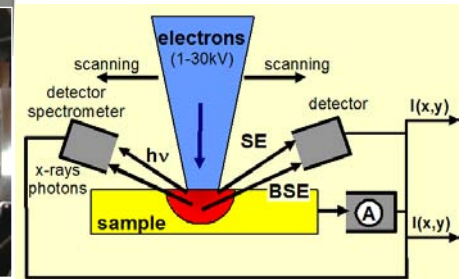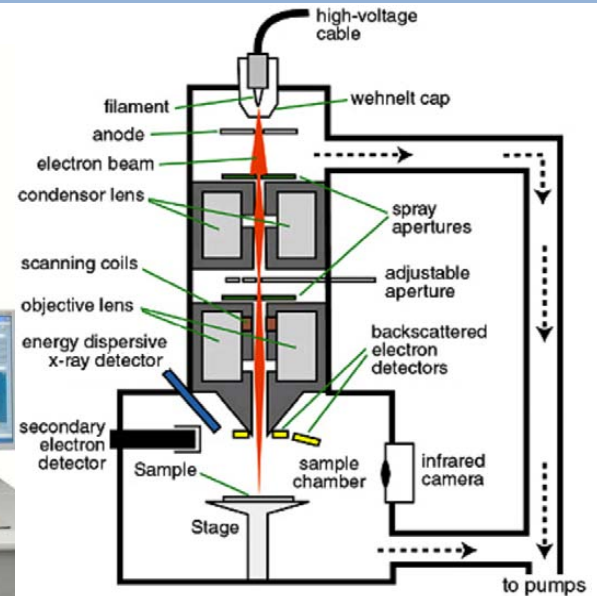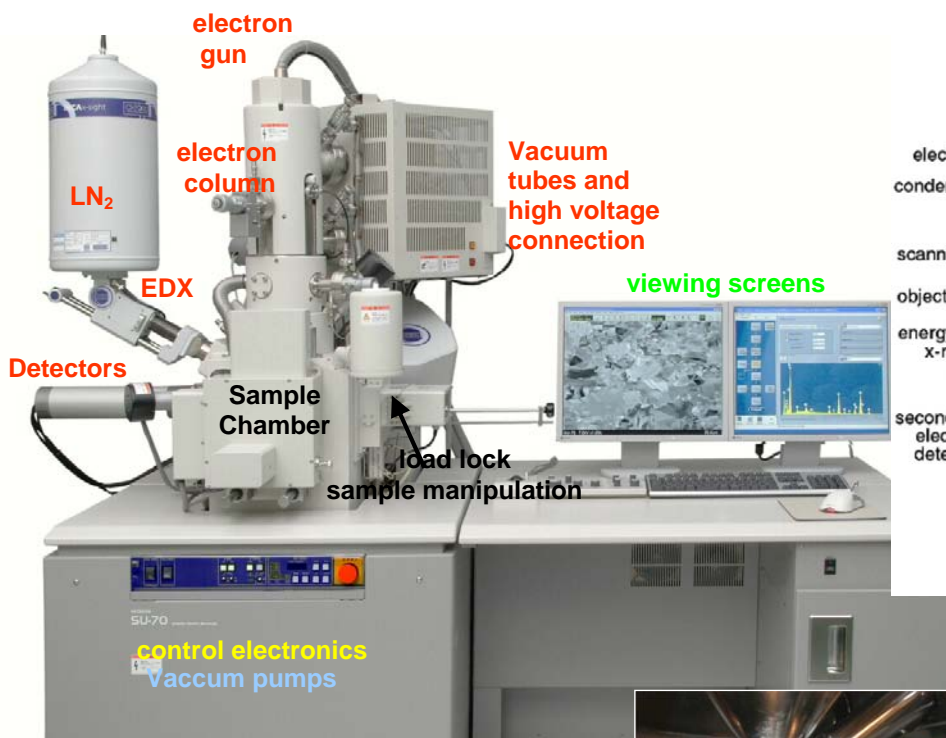
7.5.2 Resolution Factors

In SEM, the lateral resolution is determined by three main factors:

1. The **diameter of the focused electron beam spot size** d_{probe} on the sample, given by:

$$d_{probe} = \sqrt{d^2_{geometrical} + d^2_{diffraction} + d^2_{abberation}}$$

It is determined by the combination of the geometrical spot size d_{geom} as well as the diffraction and abberation broadening d_{diff} and d_{aberr} . These depend on the beam current, aperture angle, lens aberrations, electron energy and wavelength, gun brightness, …..

Note: The **minimal probe size** represents the *ultimate resolution limit* **of SEM**
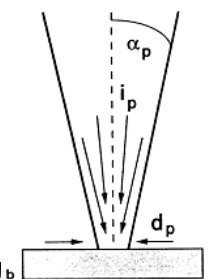
2. The **size of the interaction volume** from which secondary electrons and other signal are generated. The interaction volume increases with increasing electron energy and decreasing mass density and Z number of the sample material.

3. **Signal-to-noise noise ratio** (~probe current), **sample contrast, detection mode and efficiency**, type of detector and energy filtering of secondary signals.

$\Rightarrow$ Points #2 and #3 define the *practical resolution limit*.
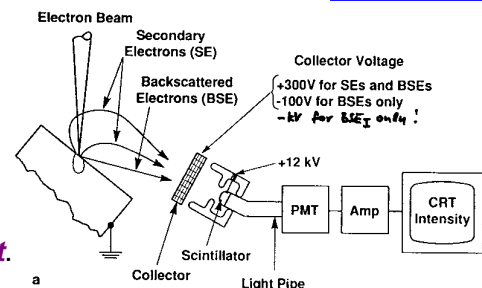
The **SEM lens system** produces a *small electron spot size with diameter d_{probe}* on the sample surface by **demagnification** of *the initial beam diameter d_0* at the cross-over within the gun onto the sample using a multiple electron lens system. Thereby, the beam is reduced to a very small size.

Electron gun (thermionic)

Demagnification Optics
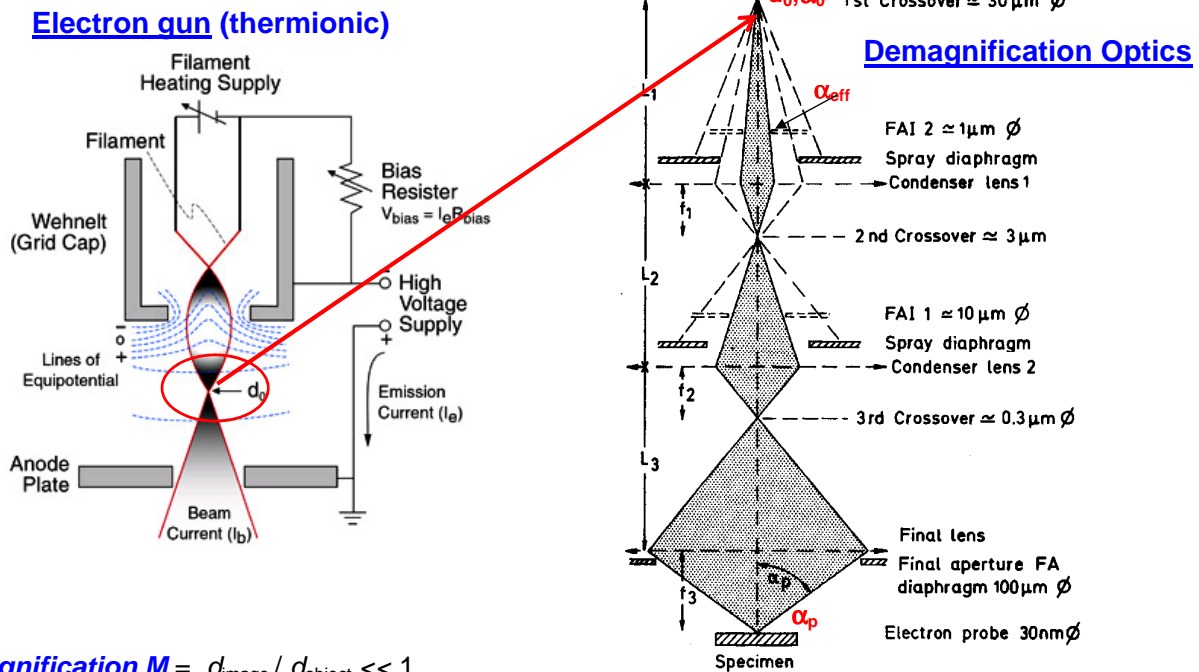
Fig. 2.13. Schematic ray in the electron-optical column of a SEM (FAI = final aperture image)

Demagnification M = $d_{\text{image}} / d_{\text{object}} \ll 1$.

For *one lens*: $M = d_{im} / d_{ob} = L_{im} / L_{ob} = \alpha_{\text{out}} / \alpha_{\text{in}} \approx f / L$

Resulting *geometrical spot size d_{geom}* for a three-lens system:

$d_{\text{geom}} = m_1 \cdot m_2 \cdot m_3 \cdot d_0 = M_{tot} \cdot d_0 \approx f_1\, f_2\, f_3 / (L_1\, L_2\, L_3) \cdot d_0$

where d_0 is the initial crossover size of the electron gun.

Thermionic guns: d_0= 50–100 µm, field emitters: d_0~10 nm

⇨ **Typical demagnifications**: M = 1/50000… 1/10.

Resulting Probe Current I_{probe}

Due to the **final aperture α_p**, actually only *a small part* of the initial electron emission cone is projected onto the sample. This strongly reduces the probe current I_{probe}.

The actual *effective emission cone* α_{eff} of electrons emitted from the source focused onto the sample is given by:

$\alpha_{eff} = m_1 \cdot m_2 \cdot m_3 \cdot \alpha_p$

Thus: $\alpha_{eff} = M \cdot \alpha_p$

$d_{geom} = M \cdot d_0$

Demagnification Optics
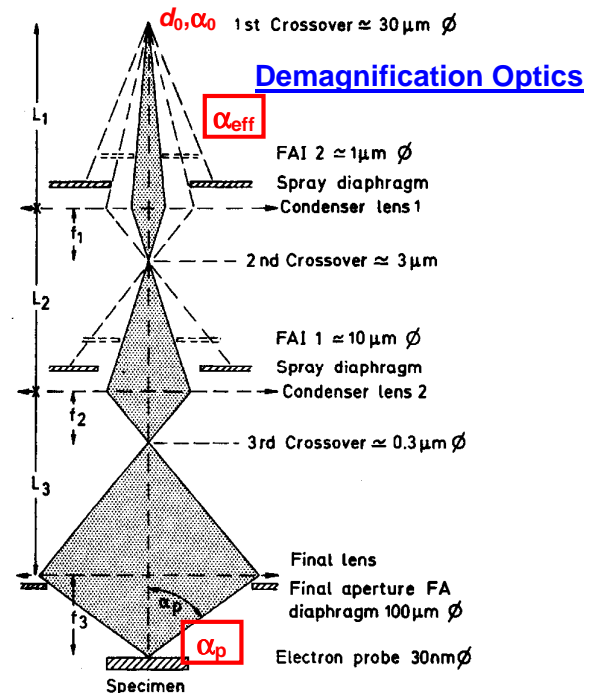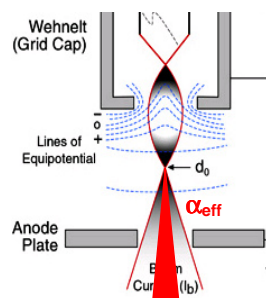
Fig. 2.13. Schematic ray in the electron-optical column of a SEM

⇨ Reducing the magnification M to achieve a small spot size simultaneously decreases the probe current !

Example: Typical working distance WD = 10 mm (~ f_3) and typical objective diaphragm diameter: 50 … 100 µm.
⇨ Final aperture: α_p = 5 - 10 mrad (0.2°) yields effective source aperture: $\alpha_{eff} \sim 10^{-4}$ mrad !!

Relation between probe current, final aperture and geometrical spot size

As shown above, the final aperture limits the beam current I_p in the final probe spot d_{geom} on the sample because only a reduced cone of emitted electrons with $\alpha_{eff} < \alpha_0$ is focused onto the sample.

The ***total emission current I_0*** emitted from the electron gun is given by:

$$I_0 == j_0\ A_0 = (\pi\ \alpha_0^2 \beta) \cdot (\pi d_0^2 / 4) \quad \text{using the gun parameters}$$

d_0 = crossover diameter and *brightness* $\quad \beta = I_e / A_e \Omega = j_0 / \pi \alpha_0^2$

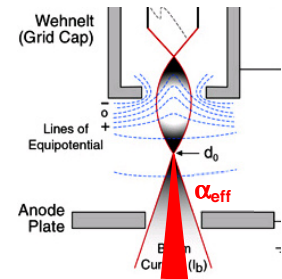The ***actual probe current I_p*** is then given by:

$$I_p = I_0 \cdot (\alpha_{eff} / \alpha_0)^2 = \pi\ \alpha_0^2 \beta \cdot \pi d_0^2 / 4 \cdot (\alpha_{eff} / \alpha_0)^2 = \tfrac{1}{4} \pi^2 \beta\ d_0^2 \alpha_{eff}^2$$

Using $\alpha_{eff} / \alpha_0 = M$ and $M = d_{geom} / d_0$ yields the relation:

$$I_p = \tfrac{1}{4} \pi^2 \beta\ d_0^2 \cdot M^2 \alpha_p^2 = \tfrac{1}{4} \pi^2 \beta \cdot d_{geom}^2 \cdot \alpha_p^2$$

⇒ Thus, the geometrical spot size and the probe current are interrelated !

$$d_{geom} = \sqrt{4/\beta} \cdot \pi \alpha_p \cdot \sqrt{I_p}$$

Conclusions:

⇒ For a given gun brightness β and final aperture α_p, the reduction of the probe diameter d_{geom} by increasing the demagnification comes at the cost of reducing the beam current I_p !

⇒ An infinitely small geometrical beam spot is achieved only with an infinitesimal small probe current !

For a required probe beam current I_p, the smallest achievable geometrical spot size d_{geom} is given by:

$$d_{geom} = \frac{\sqrt{4/\beta}}{\pi \alpha_p} \cdot \sqrt{I_p} = \sqrt{\frac{4 I_p}{\beta \pi^2}} \cdot \alpha_p^{-1}$$

Influence of the used Electron Guns

From the derived relation: $\quad d_{geom} = \dfrac{\sqrt{4/\beta}}{\pi \alpha_p} \cdot \sqrt{I_p} = \sqrt{\dfrac{4 I_p}{\beta \pi^2}} \cdot \alpha_p^{-1} \quad$ follows: $\quad I_p = \dfrac{\pi^2 \alpha_p^2}{\sqrt{4}} \cdot \beta \cdot d_{geom}^2$

⇒ Thus, for a gun with higher brightness b, a much higher beam current can be obtained for a fixed geometrical spot size !

⇒ As a result, SEMs equipped with field emission or Schottky LaB_6 guns usually provide a higher microscope performance with higher spatial resolution.

Characteristics of the Three Principal Sources Operating at 100 kV

	Units	Tungsten	LaB$_6$	Field Emission
Work function, Φ	eV	4.5	2.4	4.5
Richardson's constant	A/m^{2}K^2	6×10^5	4×10^5	
Operating temperature	K	2700	1700	300
Current density	A/m^2	5×10^4	10^6	10^{10}
Crossover size	μm	50	10	<0.01
Brightness	A/m^{2}sr	10^9	5×10^{10}	10^{13}
Energy spread	eV	3	1.5	0.3
Emission current stability	%/hr	<1	<1	5
Vacuum	Pa	10^{-2}	10^{-4}	10^{-8}
Lifetime	hr	100	500	>1000

7.5.4 Electron Spot Size due to Diffraction and Aberrations

Neglecting all other factors, the ***ultimate SEM resolution*** is given by the electron spot size d_{probe}, which is larger than the geometrical spot size d_{geom} due to diffraction and lens aberrations.

The **real final spot size d_{probe}** is given by the **root mean square sum of all broadening factors**:

$$d_{probe} = \sqrt{d_{geom}^2 + d_{diff}^2 + d_{sph}^2 + d_{chr}^2}$$

where: (see Chapter 5)

❖ d_{geom} is the geometrical spot size, given by: $d_{geom} = (4I_p / \beta\pi^2)^{1/2} / \alpha_p$

❖ d_{diff} is the diffraction broadening, given by: $d_{diff} = 0.61 \lambda / \alpha_p$
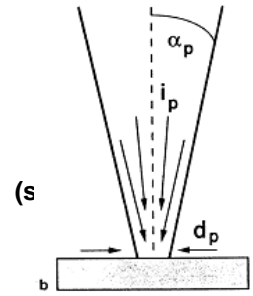
❖ d_{shp} is the spot broadening due to spherical aberration: $d_{sph} = C_{sph} \cdot \alpha_p^3 / 2$

❖ d_{chr} is the spot broadening due to chromatic aberration: $d_{chr} = C_{chr} \cdot \Delta E/E \cdot \alpha_p$

      Other lens aberrations are less important.

These factors depend on: **Objective aperture α_p, Electron energy E, Gun brightness β, Probe current I_p** and Lens properties (aberrations). Inserting the above relations yields:

$$d_{probe}^2 = \left[\frac{4I_p}{\beta\pi^2} + (0.61 \cdot \lambda)^2\right]\frac{1}{\alpha_p^2} + \left(\frac{1}{2}C_{sph}\right)^2 \alpha_p^6 + \left(\frac{\Delta E}{E}C_{chr}\right)^2 \alpha_p^2$$

❖ For small α_p, the probe diameter is inversely proportional to α_p, *i.e.*, $d_{probe} \sim 1 / \alpha_p$

❖ For large α_p, the probe diameter increases proportional to α_p^3, *i.e.*, $d_{probe} \sim \alpha_p^3$.

⇨ Thus, for a given value of the probe current I_p, gun brightness β and aberration constants $C_{shp,chf}$, there exists a certain ***optimum aperture $\alpha_{p,opt}$*** at which the ***spot size d_{probe} is minimized***.

---

(1) Dependence of the Spot Size d_{Probe} on Aperture Angle α_p

Fig. 2.14. Examples of electron-probe diameters d_p as a function of electron-probe aperture α_p for (**a**) different values of constant electron-probe current I_p using a thermionic cathode and (**b**) for 1 and 20 keV using the in-lens mode and a Schottky or field-emission gun

Cases:
- **(a) α_p and I_p small:** d_p is diffraction limited, *i.e.*: $d_p \sim 1 / \alpha_p$
- **(b) α_p small + I_p large:** d_p is limited by current I_p (d_{geom}): $d_p \sim 1 / \alpha_p$
- **(c) α_p large:** d_p is limited by spherical aberration: $d_p \sim \alpha_p^3$
- **(d) α_p intermediate:** d_p is limited by chromatic aberration: $d_p \sim \alpha_p$

(2) Dependence of d_{probe} on Beam Current I_p

$$d^2_{probe} = \left[\frac{4I_p}{\beta\pi^2} + 0.38\lambda^2\right]\frac{1}{\alpha_p^2} + \left(\frac{C_{sph}}{2}\right)^2\alpha_p^6 + \left(\frac{\Delta E}{E}C_{chr}\right)^2\alpha_p^2$$

Thus: $$d_{probe} = \frac{2}{\beta\pi\alpha_p}\sqrt{\frac{I_p}{\beta} + Const}$$

Beam Spot Size

> Smaller spot sizes d_p are obtained for red: small beam currents I_p and brighter electron guns
> (FE, LaB$_6$ - large β) !

Thermionic gun

d$_{sph}$
d$_{chr}$

I$_p$ = 10^{-10}A
10^{-11}A d$_g$
10^{-12}A
E = 20 keV
β = 7×10^4 Acm^{-2}sr^{-1}
C$_s$= 50 mm
C$_c$= 20 mm
ΔE =1 eV
d$_d$
d$_c$
d$_s$
d$_{diff}$
d$_{geom}$

a

Figure 2.24. Relationship between probe diameter d_p and probe current i_p calculated for tungsten hairpin, LaB$_6$, and field emission (FE) sources used with a pinhole lens (C_s = 20 mm, C_c = 10 mm). Curves are also shown for the FE source with an immersion lens (C_s = 2 mm, C_c = 2.5 mm). (a) Normal SEM imaging range at 30 kV. (b) SEM range at 10 kV. (c) Low-

FE gun & in-lens

C$_s$ = 4mm
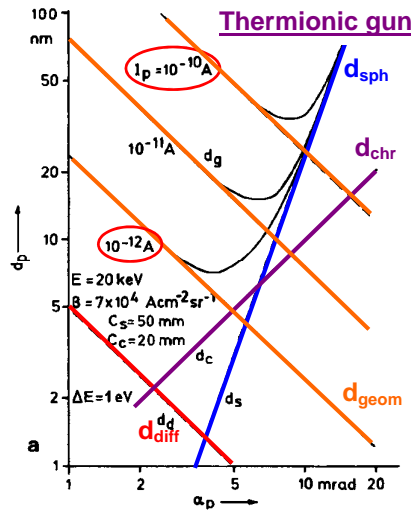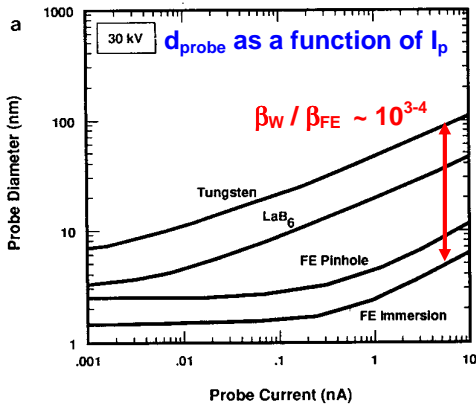C$_c$ = 2 mm
ΔE = 0,5eV
1 keV
d$_{chr}$
d$_d$
d$_c$
d$_d$
20 keV
d$_s$
d$_{diff}$
d$_{diff}$
b
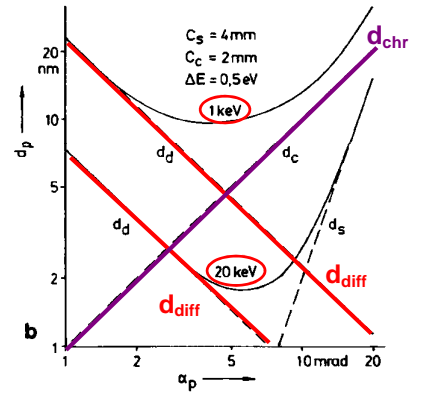
Smaller spot sizes d_p for high brightness field emitter or LaB$_6$ electron guns !

a   30 kV   d$_{probe}$ as a function of I_p
β$_W$ / β$_{FE}$ ~ 10$^{3-4}$
Tungsten
LaB$_6$
FE Pinhole
FE Immersion

---

(3) Dependence of d_{probe} on Beam Energy

$$\lambda = h/\sqrt{2mE}$$

$$d^2_{probe} = \left[\frac{4I_p}{\beta\pi^2} + 0.38\lambda^2\right]\frac{1}{\alpha_p^2} + \left(\frac{C_{sph}}{2}\right)^2\alpha_p^6 + \left(\frac{\Delta E}{E}C_{chr}\right)^2\alpha_p^2$$

with $$\lambda^2 = \frac{h^2}{p^2} = \frac{h^2}{2mE}$$

Thus, for constant current I_p and fixed aperture α_p :

$$d_{probe} \sim \sqrt{C_{const} + C_2\,1/E}$$

Consequence:

The probe size d_p decreases with increasing electron energy E, at which also the gun brightness β increases !

o **Small α_p:** d_p limited by diffraction: $C_2 = h/\sqrt{2m}\cdot 1/\alpha_p^2$

o **Large α_p:** d_p limited by chromatic aberration: $C_2 = C_{chr}\Delta E\cdot\alpha_p^2$

o **Large E:** d_p limited only by I_{probe} and by the spherical aberration constant C_{sph}.

$$d_{probe} = \sqrt{C_{const}} = \sqrt{4I_p/\beta\pi^2\alpha_p^2 + C^2_{psh}/4\alpha_p^6}$$
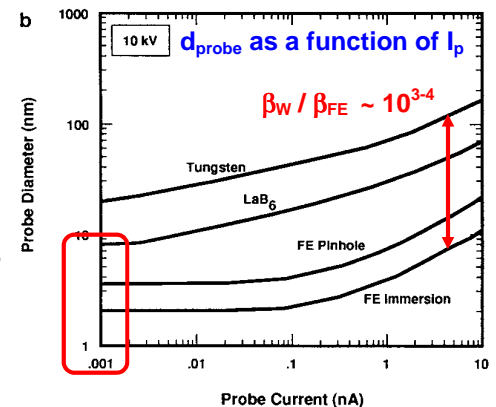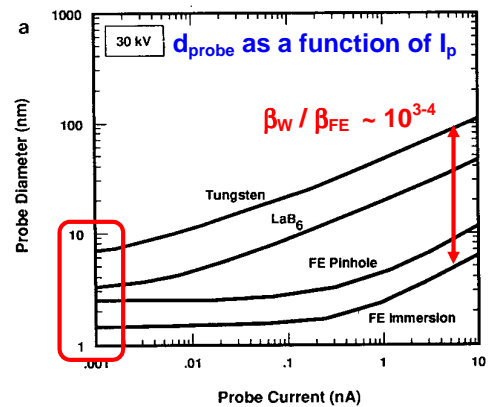
a   30 kV   d$_{probe}$ as a function of I_p
β$_W$ / β$_{FE}$ ~ 10$^{3-4}$
Tungsten
LaB$_6$
FE Pinhole
FE Immersion

b   10 kV   d$_{probe}$ as a function of I_p
β$_W$ / β$_{FE}$ ~ 10$^{3-4}$
Tungsten
LaB$_6$
FE Pinhole
FE Immersion

The probe diameter d_{probe} shows a strong dependence on the final aperture angle α_p described by:

$$d^2_{probe} = \left[\frac{4I_p}{\beta\pi^2} + 0.38\lambda^2\right]\frac{1}{\alpha_p^2} + \left(\frac{C_{sph}}{2}\right)^2\alpha_p^6 + \left(\frac{\Delta E}{E}C_{chr}\right)^2\alpha_p^2$$

For small α_p, the probe diameter is inversely proportional to α_p, i.e., $d_{probe} \sim 1/\alpha_p$ and for large α_p, the probe diameter increases proportional to α_p^3, i.e., $d_{probe} \sim \alpha_p^3$.

⇒ Thus, for a fixed value of probe current I_p, gun brightness β and aberration constants $C_{shp,chf}$, there exists a certain *optimum aperture $\alpha_{p,opt}$* at which the *spot size d_{probe} is minimized*.

Calculation of the optimum aperture angle α_{opt}:

At high electron energies (>10 kV). the chromatic aberration is smaller than the spherical aberration and can be neglected.

$$d^2_{probe} \approx \left[\frac{4I_p}{\beta\pi^2} + 0.38\lambda^2\right]\frac{1}{\alpha_p^2} + \left(\frac{C_{sph}}{2}\right)^2\alpha_p^6$$
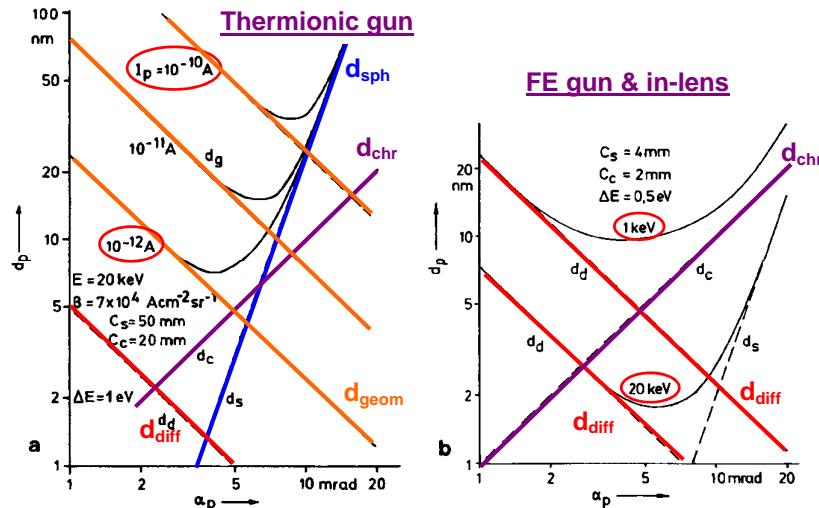
Using: $\dfrac{\partial d_{spot}(\alpha_p)}{\partial \alpha_p} \overset{!}{=} 0$, the optimum aperture angle is obtained as:

This yields: $\alpha_{opt} = \left(\dfrac{16 \cdot I_p / (3\beta\pi^2)}{C_{sph}^2}\right)^{1/8}$ with corresponding $d_{min} = \left(16 \cdot I_p /(3\beta\pi^2) + 0.38 \cdot \lambda^2\right)^{3/8} \cdot C_{sph}^{1/4}$

Usually, the geometrical spot size d_{geom} is much larger than d_{diff} and therefore, the second term in the brackets can be neglected.

Thus, $d_{min} = \left(16I_p/3\beta\pi^2\right)^{3/8}C_{sph}^{1/4}$ likewise, for a desired probe diameter the maximum allowed current is $I_{p,max} = \dfrac{3\pi\beta}{16} \cdot C_{sph}^{-2/3}d_{probe}^{8/3}$

For field emitter guns, $I_{p,max\,c}$ is given by $I_{p,max} = c \cdot d_{probe}^{2/3}$

Theoretical beam diameter limit:

In the limit of no beam current ($I_p = 0$), $d_{lim} = (4/3)^{3/8}(0.66 \cdot \lambda)^{3/4}C_{sph}^{1/4}$.

General trends: Smaller probe sizes d_{probe} can be achieved by using:

(i) higher accelerating voltages,
(ii) reduced beam currents,
(iii) electron guns with *higher brightness β* such as field emitter guns,
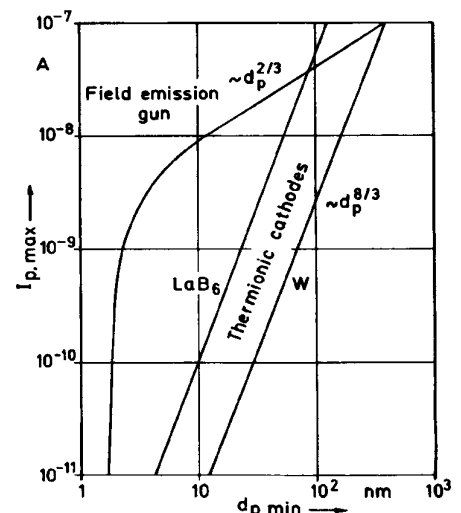(iv) *small working distances f,* which reduces the aberration constants.

Fig. 2.15. Maximum electron-probe current $I_{p,max}$ plotted against the minimum diameter $d_{p,min}$ for thermionic and field-emission cathodes

Other Factors that Influence the Practical Spot Size

Several other factors also degrade the achievable spot size:

- ❖ Alignment of gun, lenses and apertures to minimize beam distortions.
- ❖ Fluctuating electromagnetic stray fields larger than a few mGauss.
- ❖ Filament drift and misalignment.
- ❖ Charging of apertures and the samples due to electron beam induced deposition of insulating hydrocarbon layers on exposed surfaces.
- ❖ Mechanical vibrations and stability.

Thus:
$$d_{probe,eff} = \sqrt{d_{geom}^2 + d_{diff}^2 + d_{aber}^2 + d_{noise}^2 + d_{etc}^2}$$

In All:

- ➤ The smallest spot size is achieved when using: An optimum aperature, high electron energies, small probe currents, small working distances (small focal length), high brightness electron sources. Values as small as few nm can be achieved.

- ➤ The actual spot size $d_{probe,eff}$ is always *larger* than the calculated one.

- ➤ The spot size achievable with field emission guns is about 10 times smaller than for thermionic electron sources for a given probe current.

- ➤ The large interaction volume further decreases the SEM resolution but ultimately, the SEM resolution is limited by the effective probe size !

7.5.5 Depth of Field and Depth of Focus

= Depth *T* over which the image is sharp.

Criterion: Depth over which the broadening *B* introduced by being out of focus is comparable or less than the given lateral resolution *R* or spot size d_{probe}.

Broadening at an offset *T*: $B = T \cdot \tan \alpha_p = R$

Depth of field of SEM: $T = R / \tan \alpha_p$

Due to the very small aperture angles, the depth of field of SEM is two orders of magnitude larger compared to optical microscopes:

Optical Microscope: $T = \lambda / 2 \, (NA)^2 = 1.3 \cdot R^2 / \lambda$ [$\delta = 0.61 \, \lambda / NA$]

Fig. 2.25. Dependence of the depth of focus *T* on magnification *M* and resolution δ for different electron-probe apertures α_p. *Dotted line*: resolution limit due to Fig. 2.14. For comparison: depth of focus for a light microscope (LM)

At **low magnification** and **low resolution *R***:

- ➤ α_p can be chosen to be very small ~ 1 mrad.
- ➤ Therefore, depth of focus *T* is as large as 1 mm !

At **high resolution**:

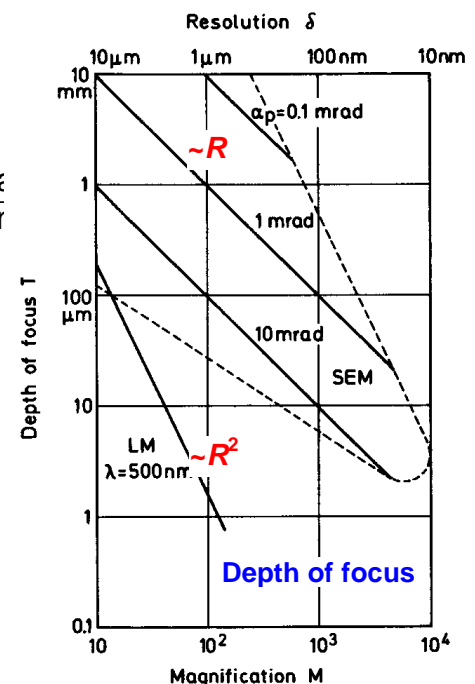- ➤ α_p ~ 10 mrad but the depth of focus is still above 2 μm !

Depth of field as a function of SEM operating conditions

Magnification	Image width $(\mu m)^a$	Depth of Field $(\mu m)^b$			
		$\alpha = 2$ mrad	$\alpha = 5$ mrad	$\alpha = 10$ mrad	$\alpha = 30$ mrad
10×	10,000	10,000	4000	2000	667
50×	2,000	2,000	800	400	133
100×	1,000	1,000	400	200	67
500×	200	200	80	40	13
1,000×	100	100	40	20	6.7
10,000×	10	10	4	2	0.67
100,000×	1	1	0.4	0.2	0.067

^{a} For a 10-cm CRT display.
^{b} $\alpha = 2$ mrad: $R_{AP} = 100\,\mu m$, $D_W = 25\,mm$; $\alpha = 5$ mrad: $R_{AP} = 100\,\mu m$, $D_W = 10\,mm$; $d = 10$ mrad: $R_{AP} = 200\,\mu m$, $D_W = 10\,mm$; $\alpha = 30$ mrad: $R_{AP} = 600\,\mu m$, $D_W = 10\,mm$.

Depth of field: Comparison of optical versus electron microscope

Optical Microscope **($T = \lambda / 2\,(NA)^2$: ~ 200nm for HR-OM)**
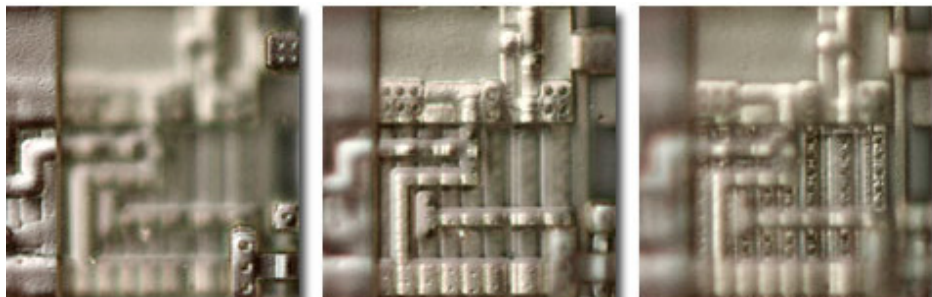
Scanning Electron Microscope **(T ~ 10 -1000 µm)**

In SEM/STEM, the **imaging signal** is essentially the **intensity of electrons emitted from the sample** due to the electron bombardment. The emitted electrons consist of two main contributions, namely,

(i) Backscattered Electrons (BSE):

   = Primary electrons backscattered from the sample with BSE_I and BSE_{II} components.

(ii) Secondary Electrons (SE):

   = Electrons excited and knocked out by the primary electrons entering the sample (SE_I) or by electrons knocked out when BSE leave the sample (SE_{II}) or by secondary processes such as x-ray photons. Practically, all emitted electrons emitted with energy less than 50 eV are considered as SE.

Escape depth Z

Due to the rather **short mean free path** λ of electrons in solids, actually **only a small fraction** of the **BSE** and **SE** electrons that are generated within a certain escape depth *Z* underneath the surface can actually escape from the sample and can be collected by an electron detector.

Escape Depth

The **escape depth Z** of electrons is about **5 times the mean free path** λ, of electrons in solids.

The **mean free path** is strongly dependent on the electron energy as shown on the right hand side.

Fig. 2.1. Universal curve of electron mean free path: experiment (Rhodin & Gadzuk, 1979; Somorjai, 1981); theory (Penn, 1976).

⇒ Essentially all emitted secondary electrons stem from a very thin layer of 5 to 50 nm

7.5.7 Spatial Distribution of Emitted Electrons

Secondary electrons with low kinetic energy: λ ~10 Å for metals, 100 Å for insulators. Z_{escape} ~10nm

Backscattered electrons with higher kinetic energies: λ ~100 Å, i.e., Z_{escape} = 50 nm.

Within each type of emitted electrons (SE or BSE), **different contributions** can be distinguished
Contributions

BSE$_I$: Localized directly backscattered electrons from single large-angle elastic scattering near the primary electron spot.

BES$_{II}$: Delocalized backscattered electrons from multiple small angle scattering events leaving the sample from more remote areas.

SE$_I$: Localized secondary electrons produced when the primary electrons enter into the sample.

SE$_{II}$: Delocalized secondary electrons produce when BSE$_{II}$ electrons leave the sample.
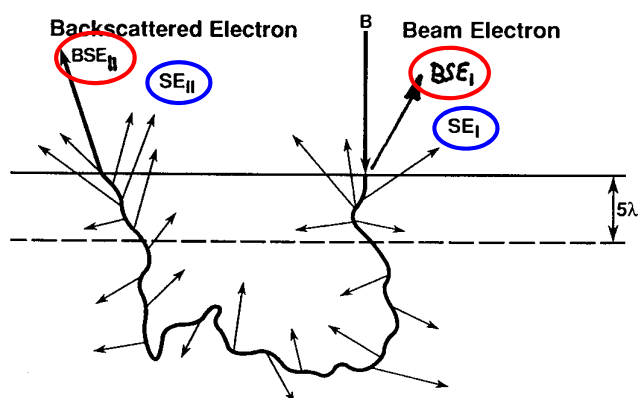

Figure 3.30. Schematic illustration of the origin of two sources of secondary electrons in the sample. Incident beam electrons (B) generate secondary electrons (SE$_I$) upon entering the sample. Backscattered electrons (BSE) generate secondary electrons (SE$_{II}$) while leaving the sample. λ is the mean free path for secondary electrons.

SE$_{III}$: There is an additional *third contribution SE$_{III}$* of *remotely generated* secondary electrons produced by electrons scattered from the inner walls of the SEM around the sample.

This creates a *nearly constant background* of secondary electrons within the SEM chamber.

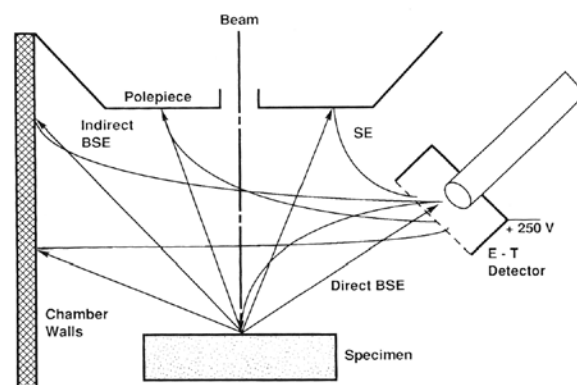All high-energy electrons within the sample chamber can produce such remote secondary electrons.

Figure 4.21. Schematic illustration of the indirect collection of backscattered electrons by a positively biased E–T detector. The backscattered electrons strike the polepiece and chamber walls, where they create secondary electrons. These secondaries are collected by the E–T detector with high efficiency. Although nominally a contribution to the secondary signal, they really represent the backscattered-electron signal component.

Example for distribution of electrons:

For Au (or C)	% of Total
• SE$_I$ – beam entering	9%
• SE$_{II}$ – BSE leaving	28%
• SE$_{III}$ – BSE (remote)	61%
• SE$_{IV}$ – Beam at apertures	2%

⇨ **SE$_I$ and BSE$_I$ electrons** are particularly important **for high resolution SEM imaging** because they come from a highly localized spot on the sample surface.

⇨ Due to their low energy of **SE$_I$** they can be efficiently collected and detected and their shallow escape depth yields high resolution and surface sensitivity.

The BSEs consists of:

(i) a strongly localized BSE$_I$ peak at primary beam spot.

(ii) a broad outer range of BSE$_{II}$ electrons.

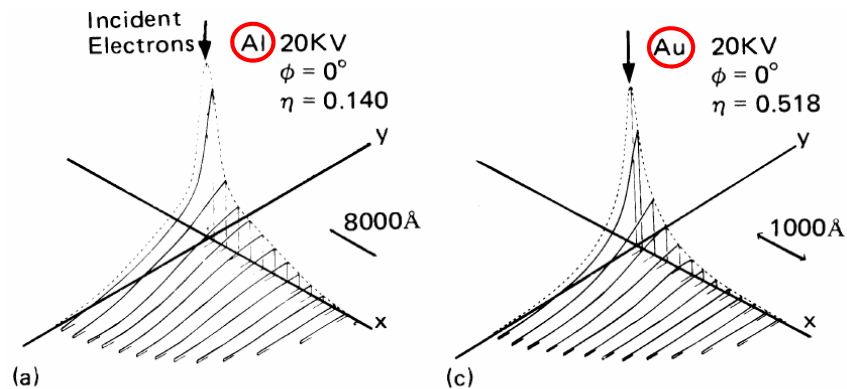(see below)
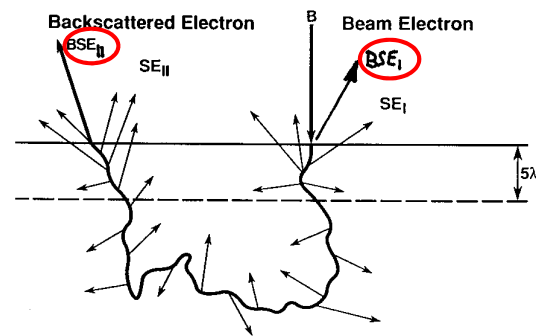
Monte Carlo Simulations:

Figure 3.23. Spatial distribution of backscattered electrons from aluminum and gold ($E_0 = 20$ keV) for 0° tilt and 45° tilt (Murata, 1974).

Lateral range of backscattered electrons

❖ **Total emission area** = R$_{BS}$ ~ R$_{KO}$ range.

❖ **But:** Majority of the BSE electrons come from much more localized spot (see prev. Fig).

❖ If one considers the range where x% of the BSE come from, this can be described as:

$$R_{BS}(x\%) = k_\% \cdot R_{KO}$$

where k$_\%$ is the cut-off proportionality factor:

Table 3.4. Cumulative Radial Backscattering (20 keV)

	k$_\%$	a. Distribution Fraction	k$_\%$
Element	80%	90%	95%
C	0.502	0.575	0.63
Al	0.419	0.490	0.545
Cu	0.318	0.382	0.439
Ag	0.250	0.310	0.365
Au	0.195	0.248	0.295
	d / R$_{KO}$	d / R$_{KO}$	d / R$_{KO}$

Both the R$_{KO}$ range as well as proportionality factor k$_\%$ decrease with increasing Z number:

⇨ **For higher Z materials, the BSE signal comes from a much smaller spot of the sample !**

Example 90%
- **For pure Al 90% of BSEs are from d/R$_{KO}$ = 0.49**
- **For pure Au 90% of BSEs are from d/R$_{KO}$ = 0.25**

Thus, 90% of the BSE signal for:
- **Au: 0.25 (0.86 μm) = 0.215 μm**
- **Al: 0.49 (4.2 μm) = 2.06 μm**

Target	Kanaya–Okayama range (μm) Beam energy (keV)			
	5	10	20	30
C	0.52	1.7	5.3	10.4
Al	0.41	1.3	4.2	8.2
Cu	0.14	0.46	1.5	2.9
Au	0.085	0.27	0.86	1.7

Lateral Distribution of Secondary Electrons

The secondary electrons consist of two contributions

SE$_I$ (SE$_{Beam}$) and **SE$_{II}$ (=SE$_{BS}$)**, with
and η = backscattering yield.

$$\delta_{tot} = \delta_B + \delta_{BS}\eta$$

⇨ The area of SE$_I$ emission is ~ beam spot size:
This yields high resolution SEM images.

⇨ The area of SE$_{II}$ emission is the same as that
for BSE$_{II}$ electrons (~R$_{KO}$).
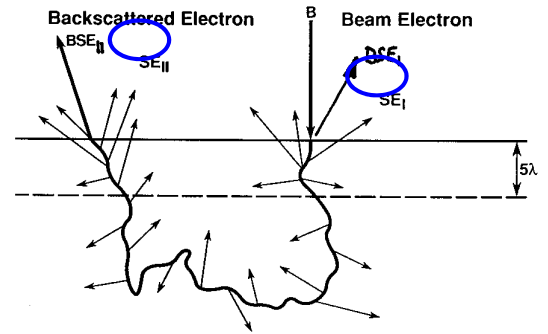
Z-dependence:

The ratio of the generation efficiency between δ_{BS} and
δ_B is about 3, but the contribution of the BS - SE$_{II}$ is
proportional to the BS yield η, which increases with
increasing Z.

⇨ Since for high Z materials R$_{KO}$ is smaller,
in principle higher lateral resolution can
is obtained for higher Z materials.

Table 3.8. Ratio of Secondary Electrons Produced by Beam and Backscattered Electrons

	δ_T	η	SE$_{II}$/SE$_I$
Carbon	0.05	0.06	0.18
Aluminum	0.1	0.16	0.48
Copper	0.1	0.30	0.9
Gold	0.2	0.50	1.5

⇨ However, the total ratio of SE$_{II}$ / SE$_I$ is proportional to the BSE yield η, which increases with
increasing Z number. Therefore, for high Z material less SE electrons come from the beam spot
on the surface and the SE current is more dominated by the low resolution SE$_{II}$ contribution.

⇨ The increase in lateral resolution for high Z materials is less pronounced than for BSE electrons.

7.5.8 Energy Distribution of Emitted Electrons and Energy Filtering

The **different electron contributions**
can be actually ***distinguished*** due to
their different ***emission energy***:

Right hand figure:

Typical ***energy spectrum***
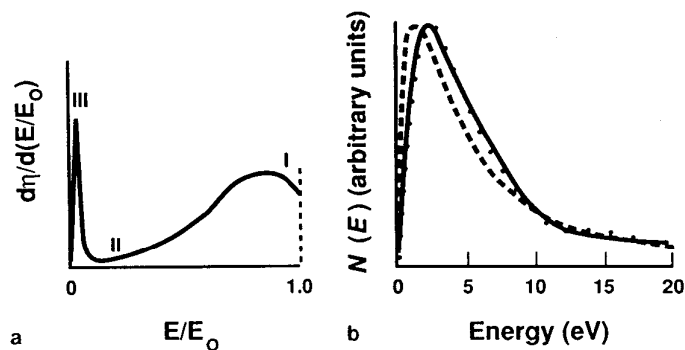of emitted electrons

Figure 3.25. (a) Complete energy distribution of electrons emitted from a target, including backscattered electrons (regions I and II) and secondary electrons (region III). Note that the width of region III is exaggerated. (b) Secondary-electron energy distribution as measured (points) and as calculated (lines) with different assumptions on secondary propagation (Koshikawa and Shimizu, 1974).

BSE$_I$: Electrons with energy close to the primary electrons (low loss electrons).

BSE$_{II}$: Electrons with intermediate energies.

SE$_{I,II,III}$: Electrons with very low kinetic energies of up to about 20 eV.

⇨ By **energy selective electron detection**, the different contributions can be ***enhanced*** or
suppressed.

⇨ This is achieved, e.g., by using an **Evenhart-Thornley electron detector**.

Energy Filtering by Electron Detectors

Evenhart-Thornley detector: For high-sensitivity detection of the small electron currents (nA) emitted from the sample, a scintillator-photomultiplier detector is used, in which the emitted electrons are first converted to photons and subsequently amplified by a high gain photomultiplier.

Energy filtering using a collector grid:

(a) **Large positive bias** (attraction of electrons):
High collection efficiency for all types of electrons. Thus, the image intensity (current) is high but the spatial resolution low.

(b) **Small negative bias** (repulsion):
Suppression of low-energy secondary electrons SE, detection only of BSE.

(c) **Large negative bias** (strong repulsion):
Collection of only the directly backscattered BSE_I electrons for high spatial resolution.
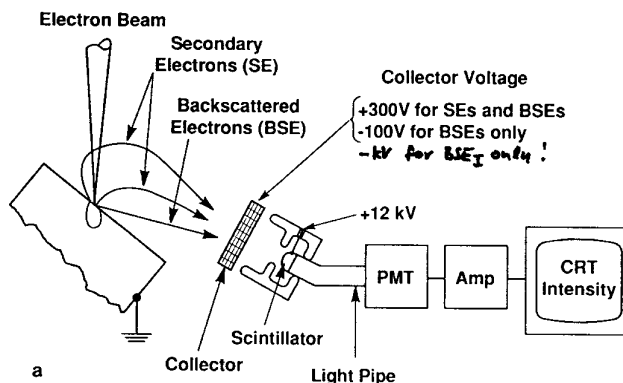
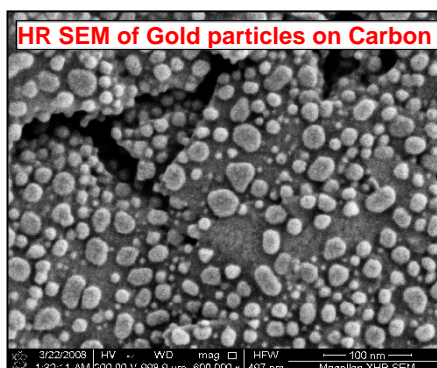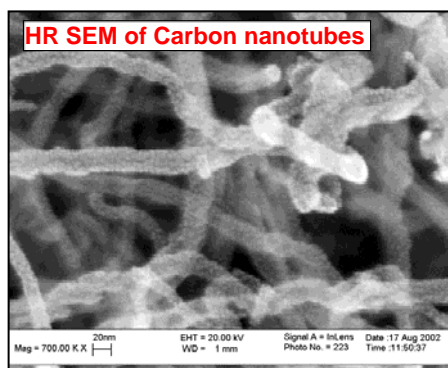**Semiconductor pn/Shottky junction detector:**
Impinging electrons create electron hole pairs, causing a current across the reversely biased pn junction. The average number of electron-hole pairs per incident electron is roughly equal to ~ E_0/E_{gap}, where E_{gap} is the semiconductor band gap.
Thus, high energy electrons give a higher signal, therefore, this dector is mainly used for **backscattered electrons**.
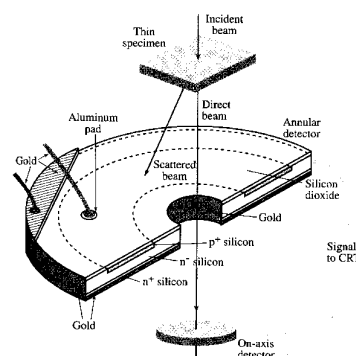
7.5.9 SEM Resolution

(1) Only directly backscattered electrons BSE_I and the secondary electrons SE_I stem from a highly localized spot around the primary electron beam spot on the surface.
  ⇨ High lateral resolution can be obtained only from these contributions!
  ⇨ Under ideal conditions, a resolution nearly equal to the probe size can be achieved.

(2) The high resolution signal is superimposed by a broad background with low resolution.
Thus, the high resolution signal-to-background ratio is often rather small and must be optimized.

  ⇨ The resolution can be enhanced by discriminating electrons using energy filtering.

(3) **Energy dependence:** At lower energies, the electron range decreases but the spot size increases.

(4) **Z dependence:** For high Z materials, the electron range decreases but the contribution from non-local BSEII and SEII increases.

Best resolution:

HR SEM of Carbon nanotubes

HR SEM of Gold particles on Carbon

coliphage

Low-loss SEM image

Increased Resolution for Backscattered Electrons by Energy Filtering

Directly backscattered electrons BSE$_I$ with very small energy loss originate from the impingement area of highly focused electron beam: » High resolution imaging possible also with BS electrons.
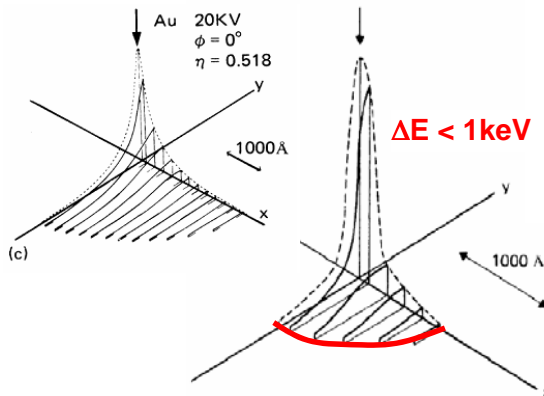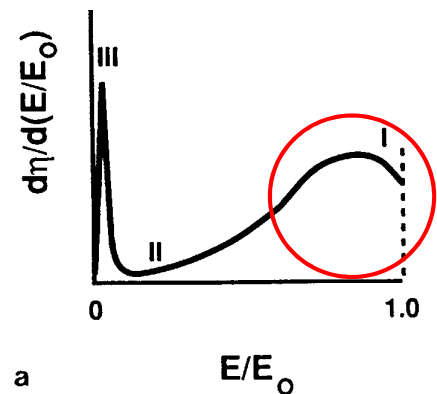
❖ **Backscattered electrons BSE$_{II}$**

Au 20KV
$\phi = 0°$
$\eta = 0.518$

1000Å

ΔE < 1keV

1000 Å

Figure 3.24. Spatial distribution of backscattered electrons which have lost less than 1 keV of energy ($E_0 = 20$ keV, $\phi = 0°$, $\Delta E < 1$ keV) (Murata, 1973).

$d\eta/d(E/E_O)$

III

II

I

0   1.0

E/E_O

a

Lateral resolution of BSE signal: $\boxed{d_{eff} = (d^2_{probe} + d^2_{BSE})^{1/2}}$ where d_{BSE} is the emission range for BSE.

- » **d_{BSE} can be strongly reduced by energy filtering** of the BSE signal by the detector.
- » **High-resolution low-loss BSE images** using negatively biased ET or semiconductor detectors.
- » But: d_{BSE} is always proportional to R_{KO}: Higher resolution achieved for larger Z and smaller E_{probe}.

7.5.10 Contrast in SEM

A. Chemical Contrast - Backscattered Electrons (BS)

The **backscattering yield η** is defined as $\boxed{\eta = \dfrac{n_{BS}}{n_0} = \dfrac{i_{BS}}{i_0}}$ n_0 = number of primary electrons

Empirical dependence of BS yield η as a function of atomic number Z (=Z-contrast): $\boxed{\eta = -0.0254 + 0.016Z - 1.86 \times 10^{-4}Z^2 + 8.3 \times 10^{-7}Z^3}$

General trends:

➤ *Increase* of η as a function of atomic number Z because Rutherford backscattering is more efficient for heavy atoms.

The backscattering η yield does *not* show a significant beam energy dependen

➤ The *contrast C* in backscattered electron images is mainly due to differences in chemical composition in the sample (but also contains some contributions of morphology) and is given by:

$$\boxed{C = \frac{S_2 - S_1}{S_2} = \frac{\eta_2 - \eta_1}{\eta_2}}$$ $$\boxed{\eta_{mix} = \sum_i \eta_i C_i}$$

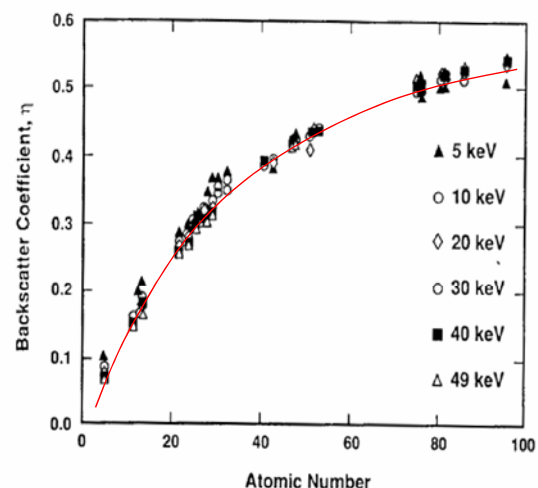C_i is the concentration of the element i within the interaction volume of the sample.

Figure 3.15. Backscattered-electron coefficient as a function of atomic number plotted for a range of beam energies from 5 keV to 49 keV [data of Bishop (1966) and Heinrich (1966a)].

Legend:
- ▲ 5 keV
- ○ 10 keV
- ◇ 20 keV
- ○ 30 keV
- ■ 40 keV
- △ 49 keV

Examples for *Z* contrast in SEM:

Ni-Cd battery element:

SE: topo | BSE: Z cotrast

Cd

Ni

50 μm

Al-Ni alloy:

$$I_{SC} = I_{probe} - I_{BS}$$

BSE electrons
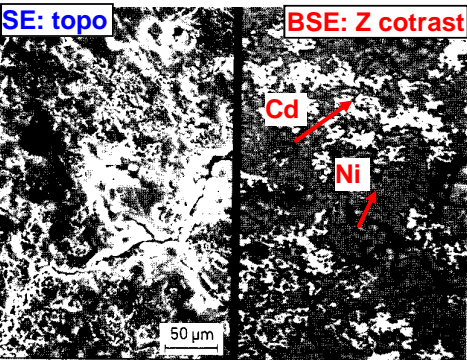
Specimen current

(a) 10μm b (b) 10μm

Figure 3-18. Secondary electron and backscattered electron images of the cathode plate of a space satellite battery. The SE image shows only the topography of the surface. The atomic number contrast in the BS image shows that Cadmium (appearing as bright particles) has redeposited across the nickel cathode (darker background).
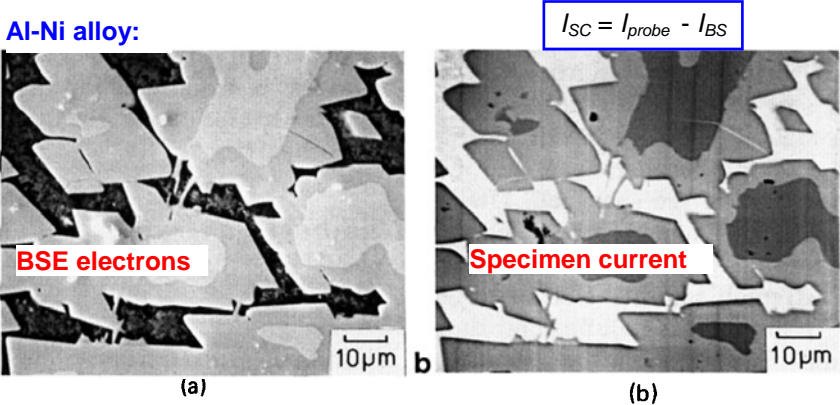
Figure 4.26. (a) Backscattered electron image derived from a reverse-biased Everhart–Thornley detector. (b) Direct specimen current image of the same region as shown in Figure 4.26a. (Note: the faint vertical lines arise from interfering stray signals.) Specimen: Raney nickel alloy (aluminum–nickel); beam energy 20 keV.

B. Topographic Contrast

Topography contrast originates from:

a) Surface tilt contrast due to dependence
of SE and BSE yields on local surface
tilt relative to electron beam.

b) Shadowing contrast due to orientation
of electron collection detector relative
to the sample surface.

c) Diffusion contrast due to enhanced
SE escape probability at step
edges.

S ~ slope

+ shadowing

roundig of edges

Table 3.8. Ratio of Secondary Electrons Produced by Beam and Backscattered Electrons

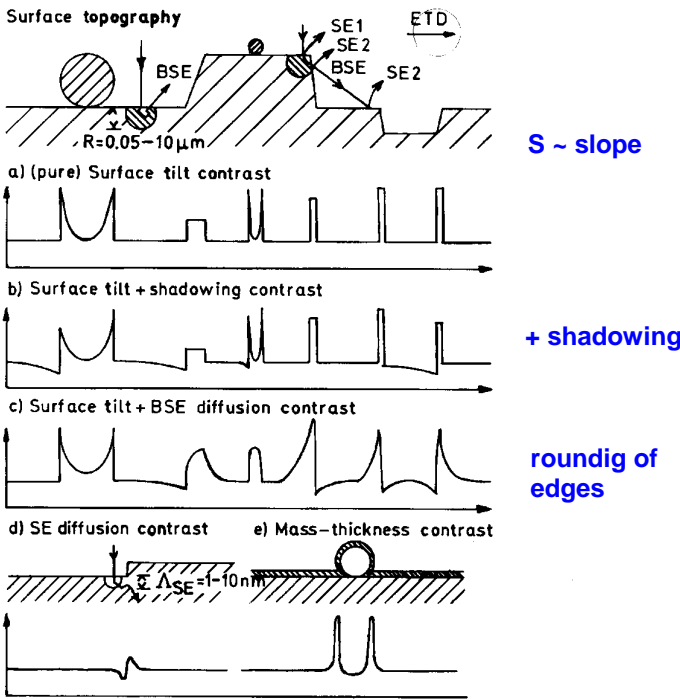|	δ_T	η	SE_{II}/SE_I
Carbon	0.05	0.06	0.18
Aluminum	0.1	0.16	0.48
Copper	0.1	0.30	0.9
Gold	0.2	0.50	1.5

Fig. 6.1. Contributions to topographic contrast demonstrated schematically by surface contours (top) and linescans of SE signals; (**a**) surface tilt contrast, (**b**) shadowing contrast, (**c**) BSE diffusion contrast, (**d**) SE diffusion contrast and (**e**) mass-thickness contrast

a) (pure) Surface tilt contrast

b) Surface tilt + shadowing contrast

c) Surface tilt + BSE diffusion contrast

d) SE diffusion contrast   e) Mass-thickness contrast

Topographic Contrast

Dependence of secondary electron yield as a function of the tilt angle θ between the primary beam and the surface normal is:

$$\delta(\theta) = \delta_0 \sec\theta$$

Origin: For grazing incident primary electrons the trajectories are closer to the surface. Thus, more secondary electrons are generated within the escape depth of the surface.

» Drastic increase of SE electron yield with increasing surface tilt angle. *Very strong topographic contrast* secondary electrons as compared to BS electrons.
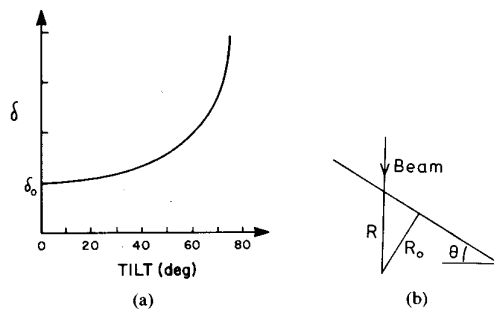
Figure 3.31. (a) Behavior of secondary-electron coefficient δ as a function of specimen tilt θ, following a secant law. (b) Origin of secant law behavior.
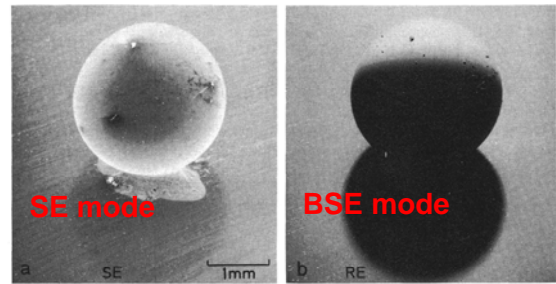
Fig. 6.2. Imaging of a 3 mm steel ball in the (a) SE and (b) BSE mode with biases of +200 V and −50 V at the collector grid of an Everhart–Thornley detector, respectively, to demonstrate the topographic contrast and the stronger shadow casting in the BSE mode
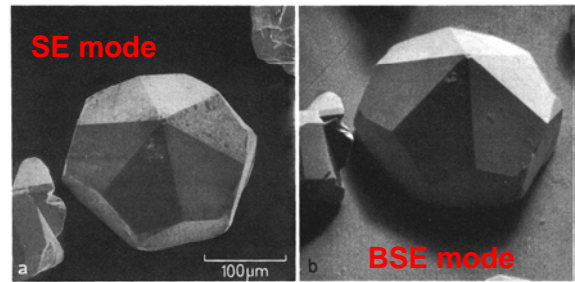
Fig. 6.3. Illustration of surface tilt and shadow contrast with micrographs of $Ge_{38}P_8I_8$ crystals in the (a) SE and (b) BSE mode

---

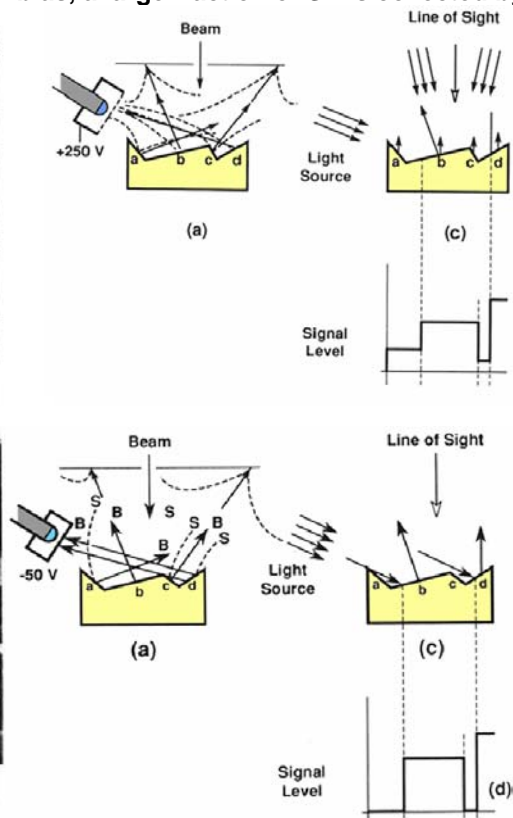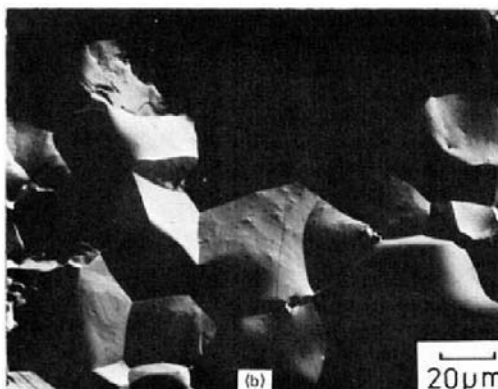# Shadowing Contrast and its Control by the Detector Bias

High-energy BS electrons: Detected only when directly hit the detector » very strong shadowing effects

Secondary SE electrons: Due to positive detector bias, a large fraction of SE is collected by the detector.

SE:
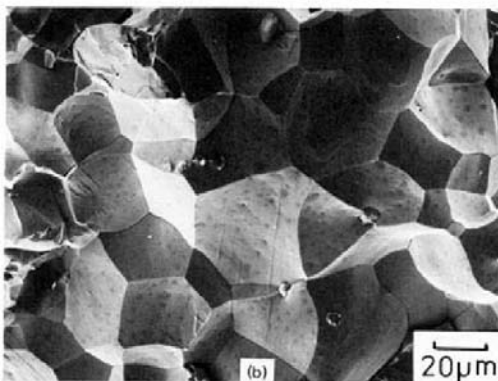
BSE:

Additional large area solid-state BSE detectors yield a high BSE collection efficiency and a BSE signal
with reduced topographic contrast:
This can be used to increase the chemical contrast and to suppress the topography contrast in the BSE images. A **segmented BSE detector** allows an additional contrast tuning.

Z-contrast: (A+B)   Topo = (A-B);

(A+B)   +SC

(A-B)   -SC

20µm   20µm   20µm   20µm
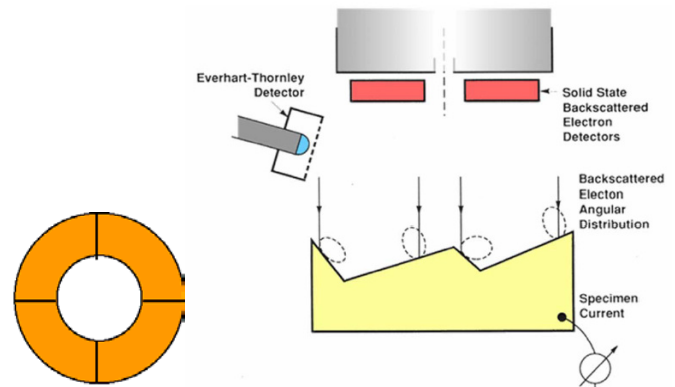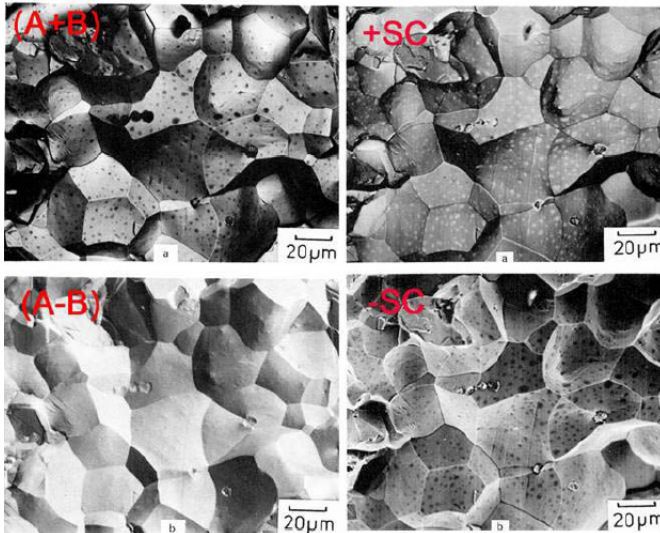
Specimen current: $I_s = I_{probe} (1 - \eta_{BS} - \delta_{SE})$:
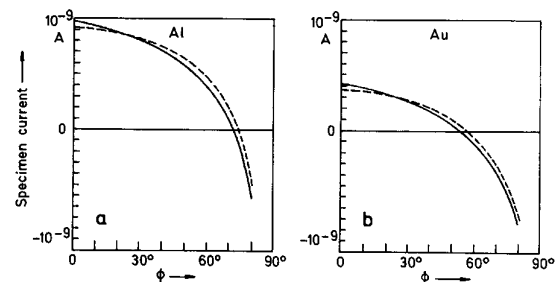**same Z dependence as BSE electrons:**

Fig. 6.18. Dependence of the specimen current on the surface tilt angle ϕ for (a) Al and (b) Au (——) experiment, (- - - -) calculated by (6.7)

7.6 Summary

❖ X-ray and electron microscopy can provide a much higher resolution due to the much shorter wavelength of x-rays and electrons compared to visible light.
However, both techniques represent cases where the actual achievable resolution is mostly limited by lens aberrations and not so much by the wavelength.

❖ **EUV and X-ray microscopy:**

The realization of EUV and x-ray microscopes is *difficult*. The reasons is region:
(i) the absorption of all materials becomes large, i.e., not transparent media are available and
(ii) the refractive index of all materials is close to one.
Therefore, no simple optical systems can be made, but complicated reflective multilayer or diffractive optics (Fresnel zone plates) must be used. Also, no simple light sources are available.

❖ **Electron microscopy:**

For electrons or charged particles, electro-magnetic lenses are used as optical elements, in which *non-uniform electric or magnetic fields* are used to obtain a focusing action.

The lens aberrations of electro-magnetic lenses are much larger than for optical lenses, and only limited aberration corrections are available.

Therefore, **resolution of electron microscopy** is mainly limited by the *lens aberrations*.

As a result an optimum aperture angle of the order $\alpha < 1°$ exists for which the resolution is maximized for a given lens system and electron energy.